The tectonic fabric of the ocean basins

Kara J. Matthews,[1] R. Dietmar Müller,[1] Paul Wessel,[2] and Joanne M. Whittaker[1]

Received 4 April 2011; revised 11 October 2011; accepted 15 October 2011; published 24 December 2011.

[1] We present a global community data set of fracture zones (FZs), discordant zones, propagating ridges, V-shaped structures and extinct ridges, digitized from vertical gravity gradient (VGG) maps. We use a new semi-automatic FZ tracking program to test the precision of our hand-digitized traces and find a Mean Absolute Deviation of less than 3.4 km from the raw VGG minima that most clearly delineate each feature, and less than 5.4 km from the FZ location predicted by fitting model profiles to the VGG data that represent the morphology of the individual FZs. These offsets are small considering gravity data only provide an approximation for the underlying basement morphology. We further investigate the origin of non-FZ seafloor fabric by combining published abyssal hill heights computed from gravity anomalies with global half-spreading rates. A residual abyssal hill height grid, with spreading rate effects removed, combined with our interpreted tectonic fabric reveals several types of seafloor fabric distinct from typical abyssal hills. Where discordant zones do not overprint abyssal hill signals, residual abyssal hill height anomalies correspond to seafloor that accreted near mantle thermal anomalies or zones of melt-depletion. Our analysis reveals several areas where residual abyssal hill height anomalies reflect pseudo-faults and extinct ridges associated with ridge propagation and/or microplate formation in the southern Pacific Ocean.

Citation: Matthews, K. J., R. D. Müller, P. Wessel, and J. M. Whittaker (2011), The tectonic fabric of the ocean basins, *J. Geophys. Res.*, *116*, B12109, doi:10.1029/2011JB008413.

1. Introduction

[2] The satellite altimetry-derived marine gravity field reveals the tectonic fabric of the seafloor, which in turn provides information about the tectonic and volcanic history of the ocean basins and enables an approximate mapping of seafloor topography at certain wavelengths [e.g., *Sandwell and Smith*, 1997]. In the past 36 years since the first radar altimeter equipped satellite was launched (GEOS-3, 1975), improvements in instrument accuracy and data processing techniques have culminated in the production of high resolution 1- and 2-min global gravity grids [e.g., *Andersen et al.*, 2010; *Sandwell and Smith*, 2009, 2005]. Although, it should be noted that only 4% of collected altimetry data are suitable for deriving gravity fields, due to sparse data coverage [*Sandwell and Smith*, 2009].

[3] *Sandwell and Smith*'s [2009] most recent global gravity grid extends to ±80.7° latitude, has 1-min resolution and enables features down to 8 km in width to be resolved. This high resolution gravity grid enabled *Sandwell and Smith* [2009] to digitize the present-day mid-ocean ridge network. These data further provide an opportunity to identify and digitize a range of seafloor features that are consequences of seafloor spreading, such as fracture zones (FZs), or of the interaction between mid-ocean ridges and the convecting mantle, such as V-shaped lineations that result from mass migration of spreading segments relative to a mesospheric framework, i.e., that are related to absolute plate motion [*Schouten et al.*, 1987].

[4] Our use of the term "tectonic fabric" refers to short wavelength seafloor features less than ~200 km in scale [e.g., *Smith*, 1998; *Gahagan et al.*, 1988] that produce gravity anomalies due to near surface mass variations. Several global tectonic fabric maps have been presented since satellite altimetry data became readily available, which focused on one or more types of gravity lineations [e.g., *Briais and Rabinowicz*, 2002; *De Alteriis et al.*, 1998; *Gahagan et al.*, 1988]. *Gahagan et al.* [1988] presented a detailed global tectonic fabric map of the ocean basins over two decades ago. They analyzed ungridded horizontal gravity gradient data to identify and digitize a variety of tectonic features on the seafloor. Here we examine the most up-to-date gridded vertical gravity gradient (VGG) [*Sandwell and Smith*, 2009] to digitize extinct spreading ridges and trace FZs and other tectonic lineations produced by seafloor spreading in the Pacific, Atlantic, Indian and Southern ocean basins. A VGG map does not produce the 90° phase shift of vertical deflections associated with the horizontal gravity gradient [*Müller and Roest*, 1992], and compared to free-air gravity it attenuates long wavelengths and enhances shorter wavelengths, producing improved signals of the tectonic fabric of the seafloor [*Wessel and Lyons*, 1997].

[1]EarthByte Group, School of Geosciences, University of Sydney, Sydney, New South Wales, Australia.
[2]School of Ocean and Earth Science and Technology, University of Hawaii at Manoa, Honolulu, Hawaii, USA.

Copyright 2011 by the American Geophysical Union.
0148-0227/11/2011JB008413

[5] Our FZs and extinct ridges data set can be combined with magnetic anomaly data to improve plate kinematic models, estimate seafloor age grid uncertainties, and identify plate reorganization events. Traces of discordant zones reveal sites of second-order, non-rigid mid-ocean ridge segmentation [*Grindlay et al.*, 1991]. Therefore, our data set provides an opportunity to study the evolution of ridge segmentation and, by combining these traces with plate reconstruction software (e.g., GPlates) and other data (e.g., hot spots, large igneous provinces), gain a deeper understanding of which factors influence their development. We have additionally digitized V-shaped lineations that can form from ridge migration due to absolute plate motion [*Schouten et al.*, 1987], or ridge propagation [e.g., *Hey et al.*, 1980; *Hey*, 1977]. "V-shaped structures" as defined by *Schouten et al.* [1987] by can be used to test absolute plate motion models in conjunction with, or as an alternative to hot spots.

[6] Abyssal hills are another major component of the fabric of the seafloor produced at mid-ocean ridges, and similarly to FZs and other lineations produced by higher-order ridge-segmentation, they preserve valuable information about spreading rate, and the thermal and lithospheric conditions active during crustal accretion, such as axial structure [*Goff et al.*, 1997]. Collectively all these structures produce roughness in the seafloor gravity field that chronicles the evolution of spreading regimes. While seafloor gravity roughness, comprising the total tectonic fabric of the seafloor, has been studied by several authors [e.g., *Whittaker et al.*, 2008; *Small and Sandwell*, 1992; *Malinverno*, 1991], a recently published abyssal hill RMS height grid [*Goff*, 2010] provides the opportunity to study abyssal hill fabric isolated from linear FZ fabrics and intraplate volcanism. We have combined our digitized gravity lineations and extinct ridges with a residual abyssal hill RMS height grid that has spreading rate effects removed, to disentangle the various components of *Goff*'s [2010] abyssal hill data, and provide a more complete analysis of the tectonic fabric of the seafloor by considering abyssal hills separately.

2. Fracture Zones and Other Seafloor Lineations

[7] Transform faults (>30 km) segment the mid-ocean ridge system, and these corridors are further subdivided by smaller offset (<30 km) non-transform discontinuities [*MacDonald et al.*, 1991]. First-order (transform faults and propagating ridges) and second-order discontinuities leave off-axis traces and therefore preserve information about the nature of mid-ocean ridge evolution, including segmentation and seafloor spreading. Third and fourth-order discontinuities present only minor segmentation and are not visible off-axis [*Grindlay et al.*, 1991].

[8] FZs are ubiquitous features on the seafloor, they are the aseismic, off-axis traces of transform faults. Due to the juxtaposition of thick and therefore strong crust (resulting from offsets >30 km, >2 Ma), transform faults are rigid, temporally stable features that do not tend to migrate along the spreading axis [*Grindlay et al.*, 1991]; consequently they record plate motion paths. FZs also retain their morphology as they age [*Sandwell*, 1984], making them valuable temporal catalogs of plate motion.

[9] The tectonic fabric of the seafloor also includes the off-axis traces of second-order discontinuities in slow-spreading regimes - "discordant zones" [*Grindlay et al.*, 1991], and V-shaped FZ-like lineations that are orientated at low to high angles to the direction of spreading. While these features do not follow tectonic flow lines, they nonetheless preserve information about the mid-ocean ridge evolution and seafloor spreading history.

2.1. Fracture Zone Types

[10] FZ morphology results from the welding together of crust of different ages, and therefore depths, during formation [e.g., *Sandwell*, 1984]. Seafloor spreading rates and mid-ocean ridge offset are therefore the main controls over FZ morphology as they determine the age offset across the FZ axis. FZ morphology is further modified by changes in plate motion [*Kruse et al.*, 1996; *McCarthy et al.*, 1996] that cause compression or tension in the transform domain [*Menard and Atwater*, 1969].

[11] FZs that form in fast spreading regimes, "Pacific-type" FZs, are characterized by an "age/depth step"; a ridge and trough structure with the trough in the older lithosphere [*Sandwell*, 1984; *Sandwell and Schubert*, 1982] (Figure 1a). Their morphology results from flexure from differential subsidence [*Sandwell and Schubert*, 1982] and thermal bending stresses [*Wessel and Haxby*, 1990; *Parmentier and Haxby*, 1986], driven by the age contrast. Fast spreading regimes, common in the Pacific Ocean, are associated with large mid-ocean ridge offsets and therefore they tend to produce much larger age contrasts across FZs, compared to slower spreading regimes that are common in the Atlantic and Indian Oceans.

[12] FZs that form in slow spreading regimes, "Atlantic-type" FZs, display a complex array of offset-dependent morphologies that are discussed in detail by *Müller and Roest* [1992]. Small to medium-offset FZs are typically characterized by a dominant central trough, akin to a graben [*Fox and Gallo*, 1986] (Figure 1a). This structure is preserved from the transform domain and results from horizontal thermal contraction [*Collette*, 1974]. *Collette* [1986] observed that medium and large-offset Atlantic-type FZs (and some Pacific-type FZs), can display an asymmetric step-like structure with a high wall on the older side of the FZ. Large-offset Atlantic-type FZs also display age/depth steps, similar to Pacific-type FZs, yet are overprinted by rough seafloor topography and/or a deep central trough [*Müller and Roest*, 1992].

2.2. Discordant Zones

[13] Discordant zones are the on- and off-axis traces of second-order discontinuities in slow spreading regimes [*Grindlay et al.*, 1991]. Unlike transform faults, second-order discontinuities are characterized by oblique fault scarps [*Sempéré et al.*, 1993] or fault bounded basins [*Fox et al.*, 1991], and shear stresses are accommodated over a much wider zone of faulting [*Grindlay et al.*, 1991]. They are non-rigid, and due to the juxtaposition of young and weak crust (from a <2 Ma offset) they migrate along the spreading axis, or oscillate, producing V-shaped or wavy traces in the seafloor [*Grindlay et al.*, 1991] (Figure 1b). This lineation type cannot be used to constrain plate motion. Note that in intermediate to fast spreading regimes, second-

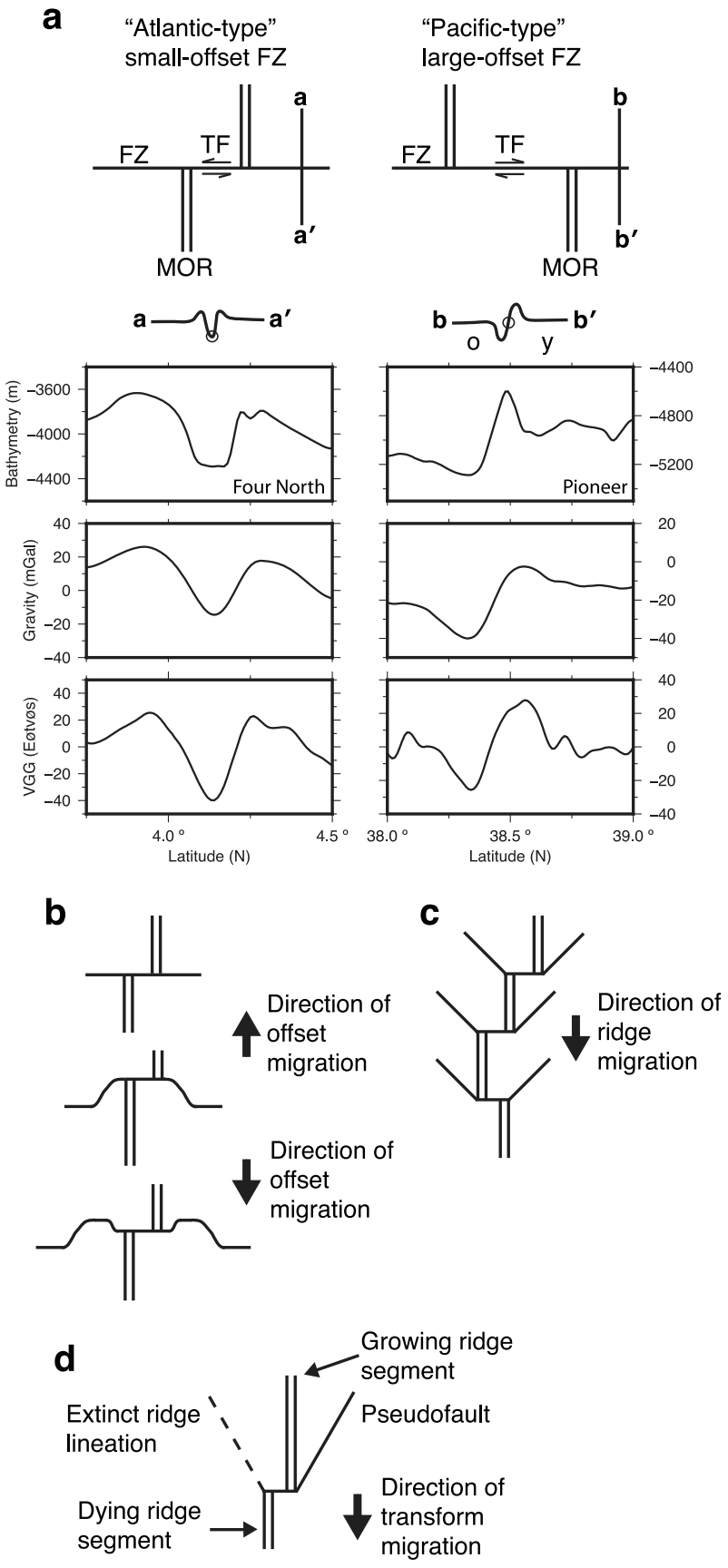
a
"Atlantic-type"
small-offset FZ
"Pacific-type"
large-offset FZ
FZ
TF
a
a′
MOR
b
b′
Bathymetry (m)
Four North
Pioneer
Gravity (mGal)
VGG (Eøtvøs)
Latitude (N)
b
Direction of offset migration
Direction of offset migration
c
Direction of ridge migration
d
Growing ridge segment
Extinct ridge lineation
Pseudofault
Dying ridge segment
Direction of transform migration

Figure 1

order discontinuities manifest themselves as "overlapping spreading centers" [*MacDonald et al.*, 1988, 1991], that can evolve into short-lived microplates [*Katz et al.*, 2005]. Based on the results of wax modeling, oblique spreading 45° to the ridge axis facilitates the microplate nucleation process [*Katz et al.*, 2005].

2.3. V-Shaped Structures and Propagating Ridges

[14] "V-shaped structures," as described by *Schouten et al.* [1987], result from spreading ridge migration driven by asthenospheric flow. They reveal absolute plate motion and can therefore be used to constrain plate kinematic models, even in the absence of hot spots [*Schouten et al.*, 1987]. These low-angle lineations should theoretically form in groups and point toward the same direction (Figure 1c).

[15] Ridge propagation involves spreading ridge tips growing along strike, and adjacent ridge segments becoming progressively extinct as the transform domain migrates in the direction of growth [*Hey et al.*, 1980; *Hey*, 1977]. As ridge tips propagate, they leave in their wake a V-shaped trail of pseudofaults on the side of the growing ridge and extinct ridge lineations on the side of the dying ridge (Figure 1d). Topographic gradients are a potential driving mechanism for ridge propagation, with propagation toward deeper seafloor [*Morgan and Parmentier*, 1985]. However, evidence from the Southeast Indian Ridge suggests that channeled asthenospheric flow along the axis of ridge segments may also play a role in ridge tip migration [*West et al.*, 1999]. This additional mechanism accounts for ridge tip propagation toward localized topographic highs [*West et al.*, 1999]. Ridge propagation is associated with first-order mid-ocean ridge segmentation [*MacDonald et al.*, 1991].

3. Methodology

3.1. Vertical Gravity Gradient (VGG)

[16] We utilized the satellite-derived gridded VGG [*Sandwell and Smith*, 2009] to locate extinct ridges, FZs and the FZ-like lineations described in Section 2. The VGG [$g_z(x) = \partial g(x)/\partial z$, where g(x) = free-air anomalies] is the second vertical derivative of Earth's potential field, i.e., the curvature (Laplacian) of the geoid. Compared to free-air gravity (the first vertical derivative of the potential field), the VGG suppresses long wavelengths and enhances shorter wavelength features such as FZs. Refer to *Sandwell and Smith* [1997, 2009] for a detailed explanation of how vertical gravity gradients are derived from satellite altimetry data.

[17] Google Earth was used to visualize v16.1 VGG tiles (the current version of *Sandwell and Smith*'s [2009] VGG data) and hand-digitize seafloor tectonic fabric elements using polyline geometries. Extinct spreading ridges were traced along their VGG minima when defined by an axial low. The Sonne ridge in the Cuvier Abyssal Plain in the eastern Indian Ocean, and the Bay of Biscay ridge comprise prominent axial highs, and we referred to *Mihut and Müller* [1998] and *Sibuet et al.* [2004], respectively, to verify their traces. Our digitization of the Magdalena ridge west of the Baja Peninsula is based on *Michaud et al.* [2006], who interpreted shipboard bathymetry and magnetic profiles; the extinct ridge and adjacent seafloor produce a complex VGG signal in this region. The FZs, second-order discontinuities and V-shaped lineations were all traced along their VGG minima, the clearest signal to identify from the gridded data. Although Pacific-type FZs are characterized by a stepped morphology, with the center of the slope delineating the FZ axis (Figure 1a), visually estimating this inflection point from the VGG maps would have resulted in too much uncertainty. Tracing the VGG minima of Pacific-type FZs ensured that their trends were preserved, as the trough in the older crust parallels the FZ scarp that marks the true FZ location [*Kruse et al.*, 1996; *McCarthy et al.*, 1996]. We chose only to trace features that produced an unambiguous signal in the VGG grids and were greater than ~100 km in length; however several ~50–100 km long oblique lineations were additionally digitized in the Atlantic due to their clarity.

3.2. Additional Data Sets

[18] A suite of additional data sets was employed to verify the locations and trends of the digitized traces. This was essential in areas where the VGG signal was weak and therefore the lineations less clearly defined. This step of comparing the VGG signal with independent data enabled us to extend the traces as far as possible, maintaining their continuity. The following supporting data sets were used: free-air gravity anomalies [*Sandwell and Smith*, 2009], bathymetry [*Smith and Sandwell*, 1997], Global Multi-Resolution Topography (GMRT) data [*Ryan et al.*, 2009], and potential field tilt [*Miller and Singh*, 1994] computed from *Sandwell and Smith*'s [2009] gravity grid. The reprocessed, retracked gravity field of *McAdoo and Laxon* [1997] enabled us to delineate FZs in areas of the Southern Ocean where sea-ice coverage reduces reliability of satellite altimetry recordings. Finally, the seafloor age grid of M. Seton et al. (Global continental and ocean basin reconstructions since 200 Ma, submitted to *Earth Science Reviews*, 2011) provided a guide as to the expected orientation of the FZs, that is, perpendicular to seafloor isochrons.

Figure 1. (a) Plan view of an (left) Atlantic- and (right) Pacific-type FZ. Two idealized VGG cross-profiles (a-a′ and b-b′) illustrate the different signals produced by the graben-type and "stepped" morphologies, respectively, with small circles showing the FZ location for each example ("y" and "o" denote the young and old sides of the large-offset FZ). Note that in this study Pacific-type FZs were traced along their trough as this is the clearest VGG signal to identify (see Section 3.1). Below the a-a′ and b-b′ cross-profiles are bathymetry (ETOPO2v2) [*National Geophysical Data Center*, 2006], free-air gravity [*Sandwell and Smith*, 2009] and vertical gravity gradient [*Sandwell and Smith*, 2009] cross-sections through Four North FZ in the Central Atlantic and Pioneer FZ in the North Pacific. Figures 1b–1d show plan view schematics of discordant zone, V-shaped structure and propagating ridge formation. (b) The wavy traces of discordant zones result from oscillations of the transform fault parallel to the ridge. (c) V-shaped structures, according to the model of *Schouten et al.* [1987], will likely form in groups and point in the direction of ridge migration. (d) Propagating ridges form pseudofaults from the growing spreading-ridge and extinct spreading-ridge lineations from the dying ridge. FZ, fracture zone; MOR, mid-ocean ridge; TF, transform fault.

Table 1. Data Set Classification Scheme

Category	Identification Criteria
Fracture Zones	Well defined linear VGG lows that clearly trace out plate motion, formed at a past or present mid-ocean ridge and are orthogonal to isochrons.
Fracture Zones - Less Certainty	FZs with very weak to absent VGG signals. In instances where there is no clear VGG signal they are identifiable in Gaussian filtered VGG data, and in the Southern Ocean they are identifiable in the retracked free-air gravity grid of *McAdoo and Laxon* [1997].
Discordant Zones	Unstable FZ-like lineations that form V-shaped and irregular wavy gravity lows. They are the off-axis traces of second-order discontinuities and clearly show evidence of offset migration back and forth parallel to the mid-ocean ridge [*Grindlay et al.*, 1991].
V-Shaped Structures	Linear gravity lows that form a low-angle 'V' at the mid-ocean ridge. Locations are taken from *Müller and Roest* [1992], who compared the orientation of V-shaped structures in the North Atlantic to the pattern of ridge migration expected from a combination of relative and absolute plate motion models, in order to confirm if they were produced by absolute plate motion.
Propagating Ridges	V-shaped pairs of pseudofaults and extinct ridge lineations that generally occur at a high-angle to the mid-ocean ridge. Atlantic and eastern Pacific traces are from *Morgan and Sandwell* [1994].
Unclassified V-Anomalies	Linear gravity lows that trace out a 'V' shape at present-day mid-ocean ridges, or would do so if reconstructed to the time of formation. Additional information is needed to enable classification as V-Shaped Structures, Propagating Ridges or Discordant Zones.

3.3. Classification Scheme

[19] Our data set comprises six classes of FZs and FZ-like structures (Section 2), as well as extinct ridges. Our rationale for categorizing the ridge-borne traces is that each feature reveals different tectonic processes and therefore the individual data sets can have different applications. For example FZs and *Schouten et al.*'s [1987] V-shaped structures enable constraints to be placed on relative and absolute plate motion, respectively. Where we were unable to determine the driving mechanism of V-shaped anomalies, we classed them as Unclassified V-Anomalies. We further qualitatively subdivided our "typical" FZ traces based on the strength of the FZ VGG signal, and how confident we were of the trace. Our classification scheme and selection criteria are described in Table 1.

3.4. Evaluating the Precision of VGG Traces

[20] We have used a new semi-automatic FZ tracking program (P. Wessel et al., manuscript in preparation, 2011) to quantify the precision of our hand-digitized FZ traces. This program tracks FZs through *Sandwell and Smith*'s [2009] VGG grid using hand-digitized VGG minima as guide points. Hand-digitized FZs are required to guide the program by defining narrow regions of seafloor within which the program will search for a FZ signal. Essentially they indicate approximately where on the seafloor a FZ should be located so that the program can better define its path.

[21] P. Wessel et al.'s (manuscript in preparation, 2011) FZ tracking program constructs a series of VGG profiles perpendicular to each FZ trace and fits model profiles to the data. The model profiles comprise a blend of (1) a symmetric (Atlantic-type) signal (Figure 2a), (2) an asymmetric (Pacific-type, age-depth step) signal (Figure 2b), and (3) a "compression"-type signal that enhances trough-flanking highs (Figure 2c). These model FZ profiles are Gaussian functions and their first and second derivatives, respectively. For each profile the program performs a nonlinear inversion to determine the optimal parameters (i.e., amplitude, width, the relative weights of the Gaussian components) then indicates the best FZ location that corresponds to each model curve, and reveals its offset from the original hand-digitized location. Additionally the FZ tracking program locates the raw VGG minimum on each profile.

[22] We selected a total of 20 Atlantic- and Pacific-type FZs for analysis using the FZ tracking program. We constructed 80 km profiles sampled every 2 km, with 10 km

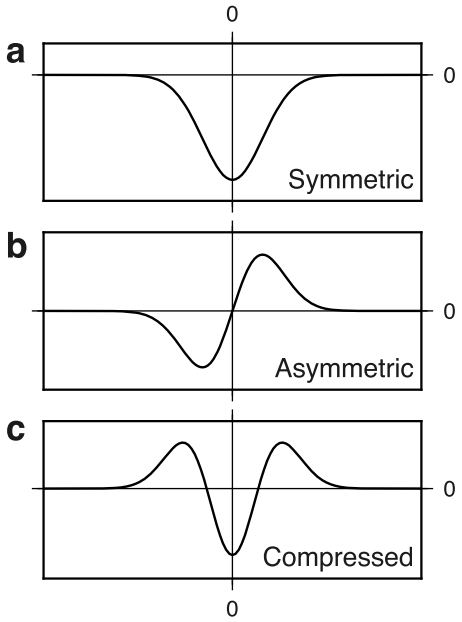

Figure 2. Gaussian-derived functions that are blended to produce best fit FZ models for the raw VGG signal. (a) Symmetric Atlantic-type signal. (b) Asymmetric Pacific-type signal. (c) Symmetric signal that has been compressed to emulate trough-flanking highs.

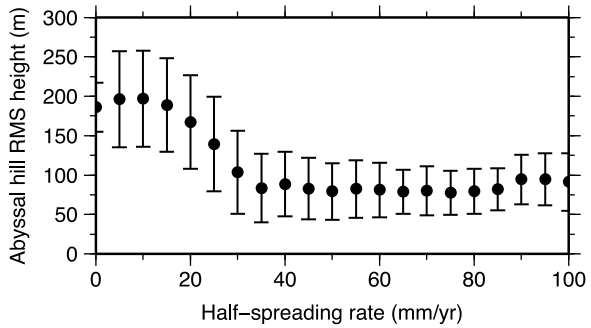

Figure 3. Median abyssal hill RMS heights as a function of half-spreading rate, calculated in 5 mm/yr bins. Error bars show median absolute deviation.

spacing between profiles. For each profile we specified a search range of 20 km, meaning that the program would only search for the best FZ location over a distance of 10 km to either side of the original hand-digitized FZ. For each FZ we computed the offset between the original hand-digitized trace and the raw VGG trough; the site we aimed to trace (see Section 3.1). Additionally, for the Pacific-type FZs we calculated the offset between the hand-digitized trough and the position of the maximum slope of the FZ scarp that actually defines this type of FZ.

3.5. Computing Residual Abyssal Hill RMS Heights

[23] *Goff* [2010] computed a predicted abyssal hill RMS height grid from small-scale gravity roughness data that he corrected for altimeter noise, by establishing how water depth and sediment thickness modify the upward continued abyssal hill free-air gravity signal. To isolate abyssal hill fabric, seafloor features such as spreading ridges, large igneous provinces and seamounts were first masked, and FZ and second-order discontinuity signals were removed via directional filtering [*Goff*, 2010]. Following the workflow of *Whittaker et al.* [2008], we produced a residual abyssal hill RMS height grid by removing the effects of spreading rate from *Goff*'s [2010] gravity-derived abyssal hill RMS height grid. This allows seafloor fabric distinct from typical abyssal hills to be located, for example that accreted near mantle thermal anomalies or zones of melt-depletion.

[24] By plotting predicted abyssal hill height [*Goff*, 2010] as a function of half-spreading rate [*Müller et al.*, 2008], we find that for rates <15 mm/yr and >35 mm/yr abyssal hill height remains fairly constant with medians of ~190 m and ~76 m respectively, while between 15 and 35 mm/yr median abyssal hill height decreases with increasing spreading rate (Figure 3). This dependence on half-spreading rate over the range 15–35 mm/yr, matches the results of *Whittaker et al.* [2008] for gravity-derived seafloor roughness, computed at somewhat larger scales, as a function of half-spreading rate.

[25] For spreading rates between 15 and 35 mm/yr abyssal hill RMS height decreases approximately linearly with increasing spreading, according to the formulation:

$$y = -5.4947x + 273.7673,$$

where y is abyssal hill height and x is half-spreading rate. We used this relationship to compute a predicted abyssal hill height grid based purely on spreading rates. These results were subtracted from *Goff*'s [2010] gravity-predicted abyssal hill RMS height grid, to yield residual heights. This residual grid was interpreted in light of our gravity lineations data set in order to disentangle its various components and illustrate how our data set can aid analyses of other geophysical data sets. Compared to *Whittaker et al.*'s [2008] seafloor roughness grid, *Goff*'s [2010] abyssal hill data resolves smaller scale features and is derived from a more recent, higher resolution gravity data set [*Sandwell and Smith*, 2009; cf. *Sandwell and Smith*, 1997]. This enabled us to test the suggestion of *Whittaker et al.* [2008] that the anomalously smooth Cretaceous seafloor in the Atlantic formed by accretion from warm mantle that had been insulated by the supercontinent Pangea, and anomalously rough Cenozoic seafloor along the Atlantic and western Indian ridges was produced by accretion from a melt depleted upper mantle.

3.6. Residual Grid Artifacts

[26] The accuracy of our residual abyssal hill height grid partly reflects the accuracy of the half-spreading rate grid from which it was computed [*Müller et al.*, 2008], as well as our empirical relationship between abyssal hill heights and half-spreading rate (Figure 3). *Müller et al.* [2008] computed half-spreading rates from stage rotations from their plate rotation model, and isochron ages, with linear interpolation between isochrons. It therefore follows that our predicted abyssal hill height grid, computed from these half-spreading rates, has stage dependent resolution. This has introduced artifacts in some locations, for example sharp boundaries are seen in the final residual grid for the northern Pacific. Calculations for the Cretaceous Normal Superchron are also less well constrained due to a lack of magnetic anomalies over such a long period of time (close to 40 Myr); half-spreading rates are therefore derived from linear interpolation over this entire period, and will not resolve any changes in spreading rate that occurred during tectonic stages. Finally, in regions where our FZ traces do not match the predicted FZ locations from the *Müller et al.* [2008] age grid, small corridors of seafloor may be assigned an incorrect spreading rate and hence incorrect residual abyssal hill heights. This type of half-spreading rate grid error is only likely to produce abyssal hill height artifacts in areas adjacent to FZs where seafloor spreading rates were 15–35 mm/yr, as for spreading rates <15 mm/yr and >35 mm/yr abyssal hill heights remain fairly constant (Figure 3).

4. Comparison Between Hand-Digitized and Semi-automatically Picked FZs

[27] We analyzed the precision of 20 of our hand-digitized FZ traces using a semi-automatic FZ tracking program (P. Wessel et al., manuscript in preparation, 2011). The Four North FZ in the Central Atlantic and Udintsev FZ in the South Pacific are representative examples of Atlantic- and Pacific-type FZs, and will be discussed in detail (Figure 4) (see auxiliary material for results for all analyzed FZs).[1] Both FZs are long-lived features and produce clear signals in the VGG grid.

[1] Auxiliary materials are available in the HTML. doi:10.1029/2011JB008413.

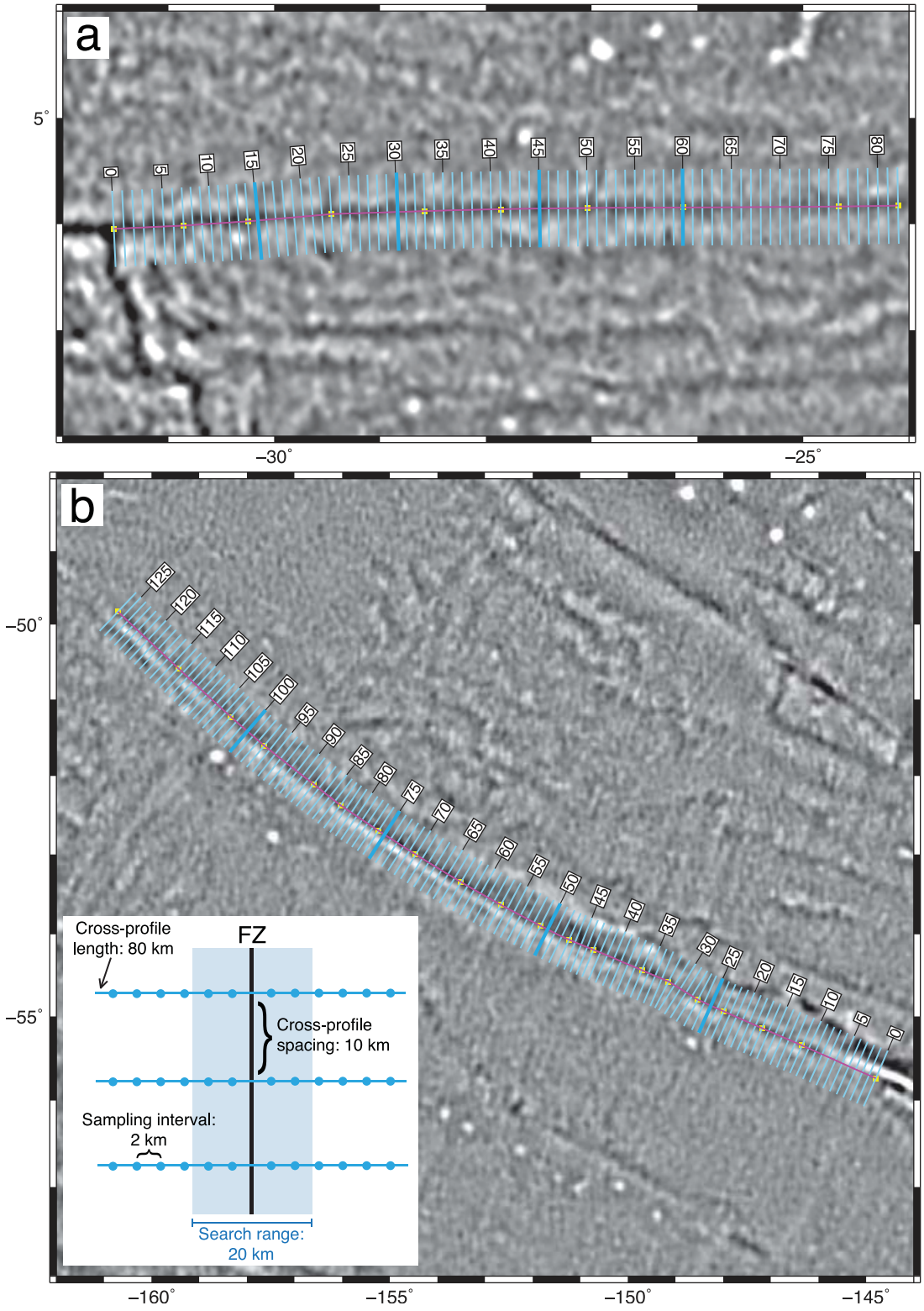

Figure 4. VGG location maps of FZs analyzed with the semi-automatic FZ tracking software (P. Wessel et al., manuscript in preparation, 2011). (a) Four North-east FZ in the Central Atlantic (North American Plate), and (b) Udintsev-west FZ in the South Pacific (Pacific Plate). FZ traces are pink on yellow, yellow squares are the hand-digitized points, cross-profiles are light blue, and profiles used in Figure 5 have been bolded. Inset shows the cross-profile specifics, with the search range (blue) as the area in which the program will search for the best FZ location.

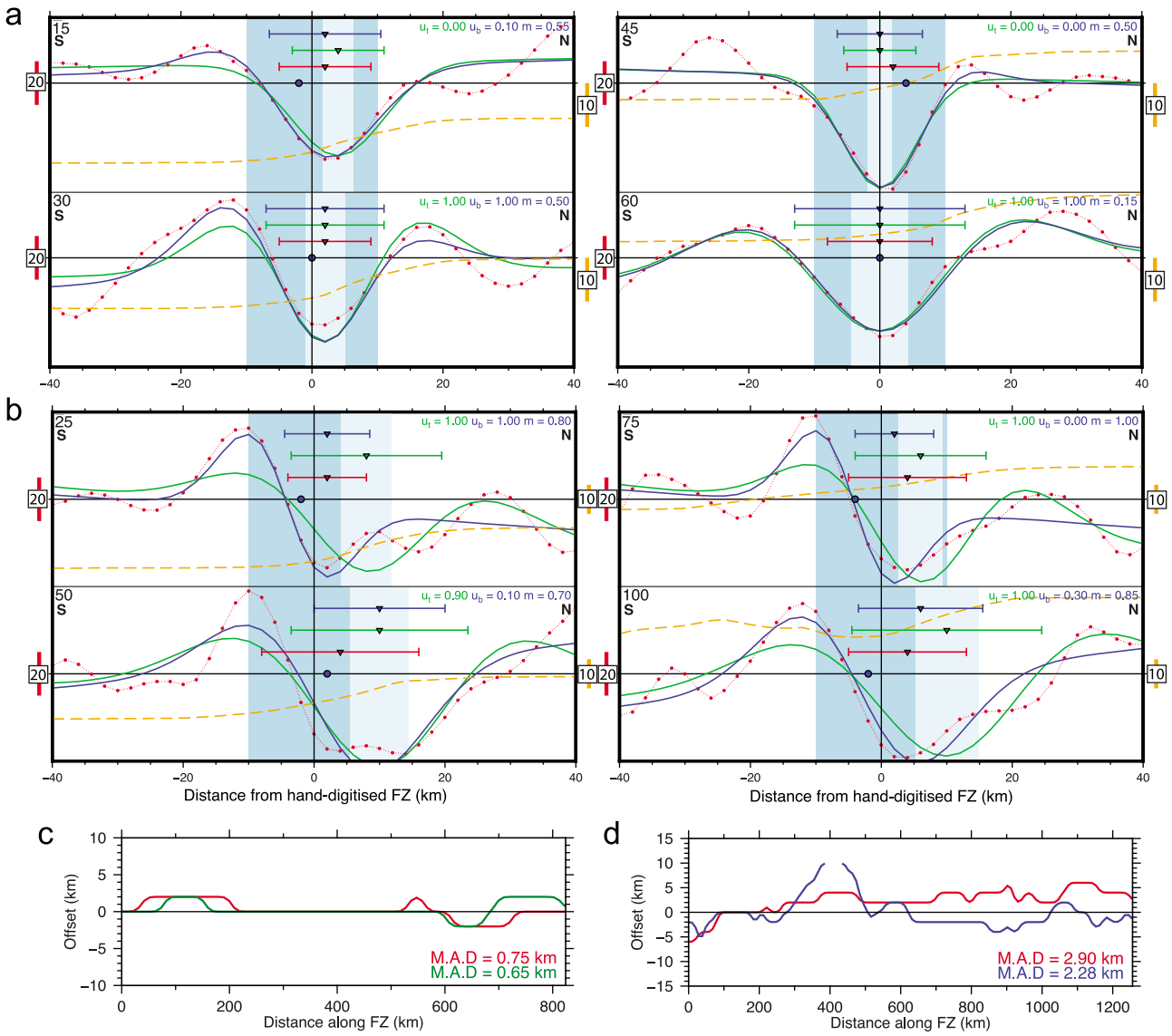

Figure 5. Results from the FZ tracking program, for the Atlantic-type Four North-east FZ in the Central Atlantic (North American Plate), and the Pacific-type Udintsev-west FZ in the South Pacific (Pacific Plate). (a, b) Cross-section plots for four equally spaced 80 km long profiles; profiles are numbered in the top left corner (see Figure 4 for profile locations). Each plot is centered on the hand-digitized FZ trace. The red curves show raw VGG data, the green curves are the best fitting trough model (comprising a blend of the symmetric Gaussian curve and its second derivative that allows for compression, see Figure 2) and blue curves are the best fitting blend model (comprising a blend of the symmetric, asymmetric and compressed symmetric curves, see Figure 2). Triangles and their error bars are color-coded to match the plotted curves and indicate the best FZ trough locations. The blue circle indicates the maximum slope location for the best fitting blend model. The dashed orange line indicates crustal age [*Müller et al.*, 2008]. The dark blue panel represents the FZ search range and the lighter blue indicates the uncertainty of the best fitting trough location (green). In the top right corner of each cross-profile the *u* values indicate the amount of compression (see Figure 2c), ranging from 0 to 1, and *m* indicates the blend between the Atlantic- and Pacific-type components; 0 indicates solely Atlantic and 1 indicates solely Pacific. Scale bar for the VGG is located to the left, and for the crustal age it is located to the right. S, South; N, North. (c, d) Offset between the hand-digitized FZ trace and raw VGG minima (red), and computed FZ locations for the Four North-east (Figure 5c) and Udintsev-west (Figure 5d) FZs. For Four North-east we additionally plot the offset between the hand-digitized FZ trace and the best fitting trough model FZ location (green) as this is an Atlantic-type FZ, and for Udintsev-west we also plot the offset between the hand-digitized FZ trace and the maximum-slope position (blue) as this is a Pacific-type FZ. If no acceptable solution is found for a profile then no offset will be plotted. M.A.D. is the Mean Absolute Deviation.

Table 2. Mean Absolute Deviation From Hand-Digitized FZ Location and Maximum Offset for Atlantic-Type FZs

	VGG Minima		Modeled Trough Position	
FZ Name	Mean Absolute Deviation (km)	Maximum Offset (km)	Mean Absolute Deviation (km)	Maximum Offset (km)
Cox-east	0.76	4	3.13	N/A[a]
Four North-east	0.75	2	0.65	2
Four North-west	0.49	2	1.3	4
Hayes-east	0.64	2	1.0	4
Kane-east	0.99	2	1.38	3.97
Kane-west	1.08	3.95	1.73	4
Martin Vaz-east	1.77	5.93	2.58	8
Martin Vaz-west	0.88	4	1.23	4
Pico	1.06	3.88	2.5	6
Vema-east	1.5	4	1.69	8

[a]For one or more profiles no offset was determined within ±10 km.

[28] Figure 5a shows 4 of the 83 profiles that were constructed perpendicular to Four North-east FZ ("-east" indicates that the trace is positioned to the east of the Mid-Atlantic ridge), spaced 150 km apart. Each profile has its origin at the hand-digitized FZ location. The red curves represent the raw VGG data and as expected they show a central trough structure that is characteristic of Atlantic-type FZs. The red triangles indicate the location of the VGG minima and reveal that for the first three profiles (profiles 15, 30 and 45) the hand-digitized troughs are offset to the south by 2 km, while for the fourth profile (profile 60) the hand-digitized FZ trough exactly matches the VGG minimum. For the entire Four North-east FZ the Mean Absolute Deviation between the hand-digitized FZ trough and the raw VGG minima (red) is only 0.75 km (Figure 5c), with a maximum offset of 2 km. The green and blue curves represent the best fitting trough and blend models, respectively, with the green and blue triangles indicating the corresponding trough locations. The blue circle reveals the location of the maximum slope of the blend model, however as Four North-east is an Atlantic-type FZ we disregard this location. The Mean Absolute Deviation of the hand-digitized trough from the best FZ location as determined by the trough model (green) is only 0.65 km (Figure 5c), with a maximum offset of 2 km.

[29] Figure 5b shows 4 of the 127 profiles that were constructed perpendicular to Udintsev-west FZ ("-west" indicates that the FZ is situated on the western flank of the Pacific-Antarctic spreading ridge), spaced 250 km apart. The raw VGG data reveal an age/depth step morphology for these profiles that is characteristic of Pacific-type FZs, and indicate that the older crust is situated to the north of the FZ as this is where the VGG trough is located. Although Pacific-type FZs are defined by the center of the age/depth step, we intentionally digitized their trough as this was the clearest signal to identify from the VGG grids. The Mean Absolute Deviation of our hand-digitized trough from the raw VGG minima (red) is 2.9 km, and from the location of the maximum slope derived from the best fitting blend model (blue) is 2.28 km (Figure 5d). The maximum offset from the VGG minima is 6 km. The maximum offset from the blend model-derived FZ trace exceeds 10 km for profiles 42–45, yet away from this part of the FZ the maximum offset remains less than ~6 km (Figure 5d). A secondary seafloor structure may be overprinting the VGG signal for this segment of the Udintsev-west FZ, particularly as the FZ Tracker is placing the maximum slope position so far to the north where the older seafloor is situated. As we hand-digitized the VGG trough it is more likely that the maximum slope position will be south of our trace, toward the younger seafloor; this is the dominant trend for the rest of the FZ (Figure 5d).

[30] Of the entire suite of 20 FZs that we analyzed, the Mean Absolute Deviation of our interpreted trough locations from the raw VGG minima remains less than 3.4 km (Tables 2 and 3). Furthermore, for the Atlantic-type FZs the Mean Absolute Deviation of our interpreted trough locations from those predicted by the best fitting trough model remains less than 3.2 km (Table 2). For the Pacific-type FZs the Mean Absolute Deviation of our interpreted trough locations from the maximum slope positions of the best fitting blend model remains less than 5.4 km (Table 3). In Tables 2 and 3 we have recorded the maximum offsets of the

Table 3. Mean Absolute Deviation From Hand-Digitized FZ Location and Maximum Offset for Pacific-Type FZs

	VGG Minima		Modeled Maximum Slope Position	
FZ Name	Mean Absolute Deviation (km)	Maximum Offset (km)	Mean Absolute Deviation (km)	Maximum Offset (km)
Clarion	2.15	8.85	2.57	N/A[a]
Marquesas	3.35	N/A[a]	2.94	N/A[a]
Menard-east	1.49	4	3.28	8
Menard-west	1.99	5.42	1.72	4
Mendaña	1.7	5.89	2.86	6
Molokai	1.83	6.52	3.18	N/A[a]
Murray	2.13	8	2.75	N/A[a]
Pioneer	2.4	N/A[a]	2.79	9.32
Udintsev-east	1.79	6	5.32	N/A[a]
Udintsev-west	2.9	6	2.28	N/A[a]

[a]For one or more profiles no offset was determined within ±10 km.

hand-digitized traces from the raw VGG minima and the model-derived FZ positions. For several FZs we were unable to compute a maximum offset, as they comprised profiles for which an acceptable solution could not be computed. This is likely due to non-FZ signals (for instance from seamounts, abyssal hills, etc.) overprinting the FZ VGG signal.

[31] *Müller et al.* [1991] examined the correlation between the short-wavelength geoid and basement topography for the Kane FZ in the North Atlantic, and found the mismatch was generally less than 10 km and 5 km on average. This indicates that while satellite derived gravity data correlate extremely well with basement topography, they do not provide a perfect spatial match. Therefore, offsets on the order of several km between our hand-digitized FZ locations and the raw VGG minima, or the modeled FZ locations, are very small and indicate that the FZs were digitized with a high level of precision. Additionally, with regards to Pacific-type FZs, *Kruse et al.* [1996] and *McCarthy et al.* [1996] noted that gravity minima generally parallel FZ scarps, and therefore digitizing a FZ from its trough preserves the trend of that FZ.

[32] Results from the semi-automatic FZ tracking program demonstrate that FZ traces cannot solely be constructed from connecting raw gravity minima, or modeled trough/FZ scarp positions as this method would produce wavy traces that do not match plate motion paths (Figures 5c–5d). The most reliable FZ traces will ultimately result from blending hand-digitized FZ locations with the FZ locations systematically extracted from gravity grids by the FZ tracking program, to produce smooth linear FZ traces that parallel plate motion. This procedure will limit bias, yet will allow for continuity when the gravity signal is weak or ambiguous. This approach will be pursued further by P. Wessel et al. (manuscript in preparation, 2011).

5. Fracture Zone and Discordant Zone Distribution Patterns

[33] FZs dominate the tectonic fabric of all ocean basins (Figure 6). The major distribution pattern is: dense spacing in slow spreading regimes (e.g., the Atlantic) and wide gaps between FZs in fast spreading regimes (e.g., the North Pacific). This reflects spreading rate influence on ridge axis morphology and segmentation. Slow spreading regimes are typically associated with short ridge segments, while the reverse is common at fast spreading ridges [*Sandwell and Smith*, 2009]. Intermediate spreading regimes are more complex, as axial morphologies are variable and display sensitivity to thermal conditions at the ridge [*Morgan and Chen*, 1993a, 1993b].

[34] The absence or disappearance of FZ traces from large swaths of seafloor is as striking as their abundance elsewhere. Sedimentation and volcanism are post-formation processes that can weaken and erase FZ signals, respectively. More localized patterns in FZ coverage appear to be associated with spreading rate and plate boundary processes including plate reorganizations.

[35] When analyzing our data set we refer to four classes of half-spreading rate: ultraslow (<6 mm/yr) [*Dick et al.*, 2003], slow (6–30 mm/yr), intermediate (30–40 mm/yr) [*Small and Sandwell*, 1992; *Chen and Morgan*, 1990] and fast (>40 mm/yr). These ranges correspond to different ridge axis and ridge flank morphologies, and sub-axial structures [*Sandwell and Smith*, 2009; *Small and Sandwell*, 1994; *Morgan and Chen*, 1993a, 1993b; *Malinverno*, 1991; *Chen and Morgan*, 1990].

5.1. Fast Spreading Pacific

[36] The highest present-day spreading rates are found along the East Pacific Rise, typically exceeding a half-spreading rate of 50 mm/yr, and reaching >70 mm/yr [*DeMets et al.*, 2010]. Similar fast spreading rates existed between the Pacific and Farallon plates during the Cretaceous and Cenozoic [*Müller et al.*, 2008], yet FZ distribution trends are very different between the two regions. Pacific-Farallon FZs, north of Marquesas FZ and trending approximately N80°E (Figure 6a), produce strong gravity signals and are continuous for over several thousand kilometers. Spacing between the major FZs generally exceeds 700 km, although individual multistrands within a FZ suite may be separated by less than 40 km (e.g., Molokai FZ). The inter-FZ corridors are typically characterized by low amplitude abyssal hill topography [*Goff*, 2010], and an absence of other FZ-like lineations. Along the East Pacific Rise FZs are similarly spaced at intervals >500 km near the Bauer microplate ('BMP' - Figure 6a), however in contrast to the Pacific-Farallon FZs in the North Pacific, there are fewer and their gravity signals are less clear and continuous (Figure 6a). Second-order segmentation dominates the East Pacific Rise with discontinuities in the form of overlapping spreading centers [*Naar and Hey*, 1989; *Lonsdale*, 1989; *MacDonald et al.*, 1988]. The East Pacific Rise is also associated with the active Juan Fernandez, Easter and Galapagos microplates (Figures 6a and 6b). It is plausible that a similar mid-ocean ridge configuration, dominated by overlapping spreading centers, once existed along the early Pacific-Farallon ridge, however the off-axis evidence of higher-order ridge segmentation has since been subducted or obscured by sedimentation and volcanism.

5.2. Slow and Ultraslow Spreading Regimes

[37] The typical pattern of dense FZ spacing at the slow spreading Mid-Atlantic, Southwest Indian and Northwest Indian ridges, is combined with wide FZ bounded corridors, 300 to >1000 km in length, that are highly segmented by second-order non-transform discontinuities (Figures 6c–6f). These regions are characterized by very rough, highly crenulated seafloor [*Morgan and Parmentier*, 1995] with discordant zones that are difficult to distinguish from the VGG maps. A well-studied example from the North Atlantic exists between the Kane and Atlantis FZs [e.g., *Briais and Rabinowicz*, 2002; *Sempéré et al.*, 1993] (Figure 7a). Comparing the global distribution of discordant zone traces to half-spreading rates reveals that these highly crenulated corridors tend to form in slower slow spreading regimes, where the half-spreading rate is predominantly <15 mm/yr, for example they are more prevalent at the North Atlantic Ridge, Southwest Indian Ridge (where periods of ultraslow spreading are also recorded) and the Northwest Indian Ridge. In faster slow spreading regimes, where spreading is ~15–30 mm/yr, such as at the Pacific-Antarctic ridge (between 60 Ma and ~10–5 Ma), the South Atlantic ridge and the Southeast Indian Ridge near the Rodriguez Triple Junction, the wavy traces of discordant zones are clearer and

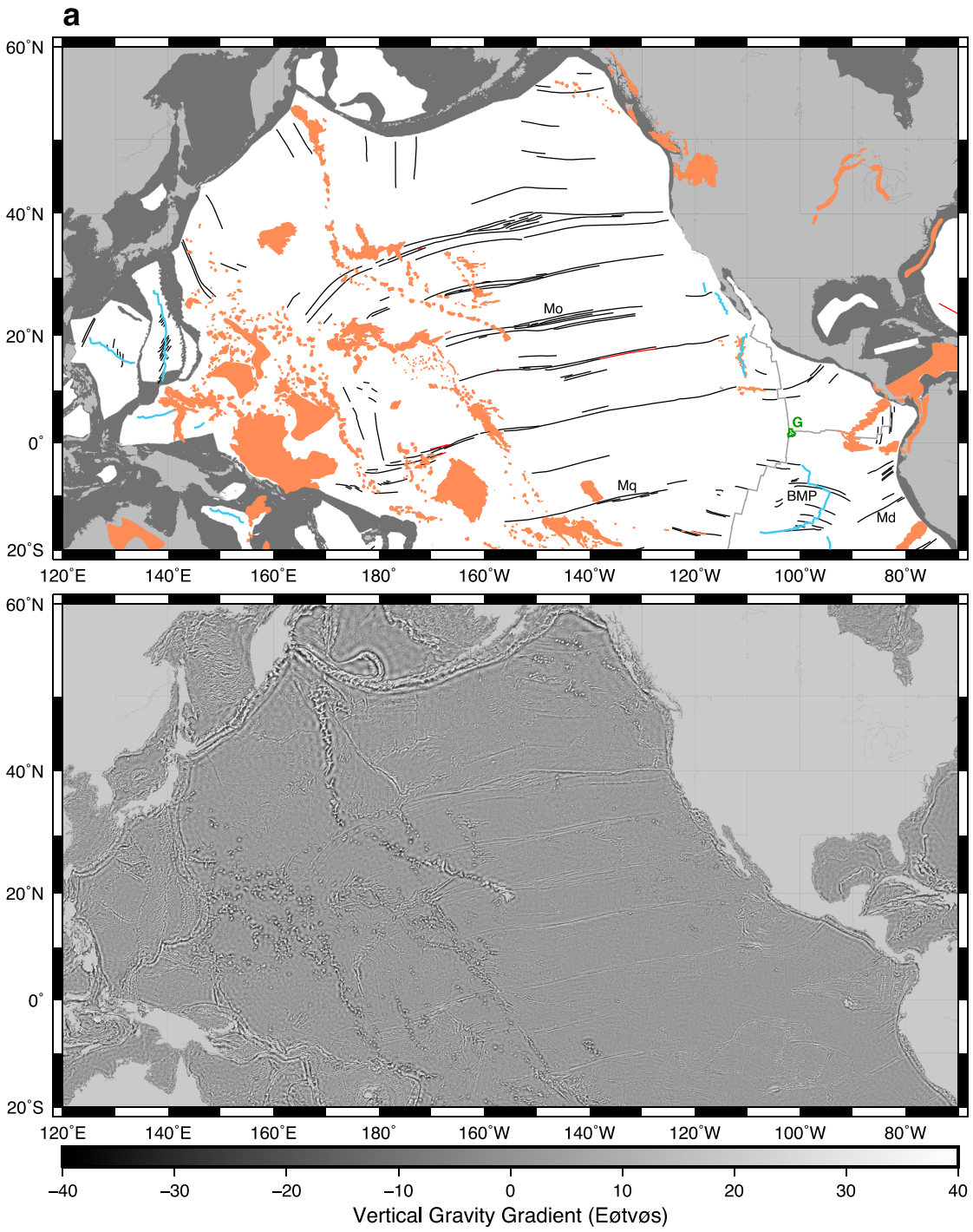

Figure 6. Tectonic fabric maps of the ocean basins: (a) North Pacific, (b) South Pacific, (c) North Atlantic, (d) South Atlantic, (e) North Indian, and (f) South Indian showing (top) digitized gravity lineations and (bottom) the VGG grid of *Sandwell and Smith* [2009]. Continental crust is shaded gray [*Müller et al.*, 2008]. Seamounts and large igneous provinces are orange [from *Coffin and Eldholm*, 1994]. Extinct ridges are light blue, FZs are black, less certain FZ traces are red, discordant zones are magenta, propagating ridge lineations are blue, V-shaped structures are orange, and unclassified V-anomalies are green. Mid-ocean ridge traces are from *Sandwell and Smith* [2009]. Abbreviation in Figure 6a are Mo, Molokai FZ; Mq, Marquesas FZ; Md, Mendaña FZ ; G, Galapagos microplate; BMP, Bauer microplate. Abbreviations in Figure 6b are E, Easter microplate; JF, Juan Fernandez microplate. In Figures 6c and 6d pink dashed lines indicate where there is a transition to fewer FZ traces, suggesting an increase in spreading rate has occurred. In Figure 6c the pink dashed line also marks the transition from rougher to comparatively smoother seafloor, again consistent with an increase in spreading rate. In Figures 6e and 6f the triangle marks the location of the Rodriguez Triple Junction. EB, Enderby Basin; WB, Wharton Basin.

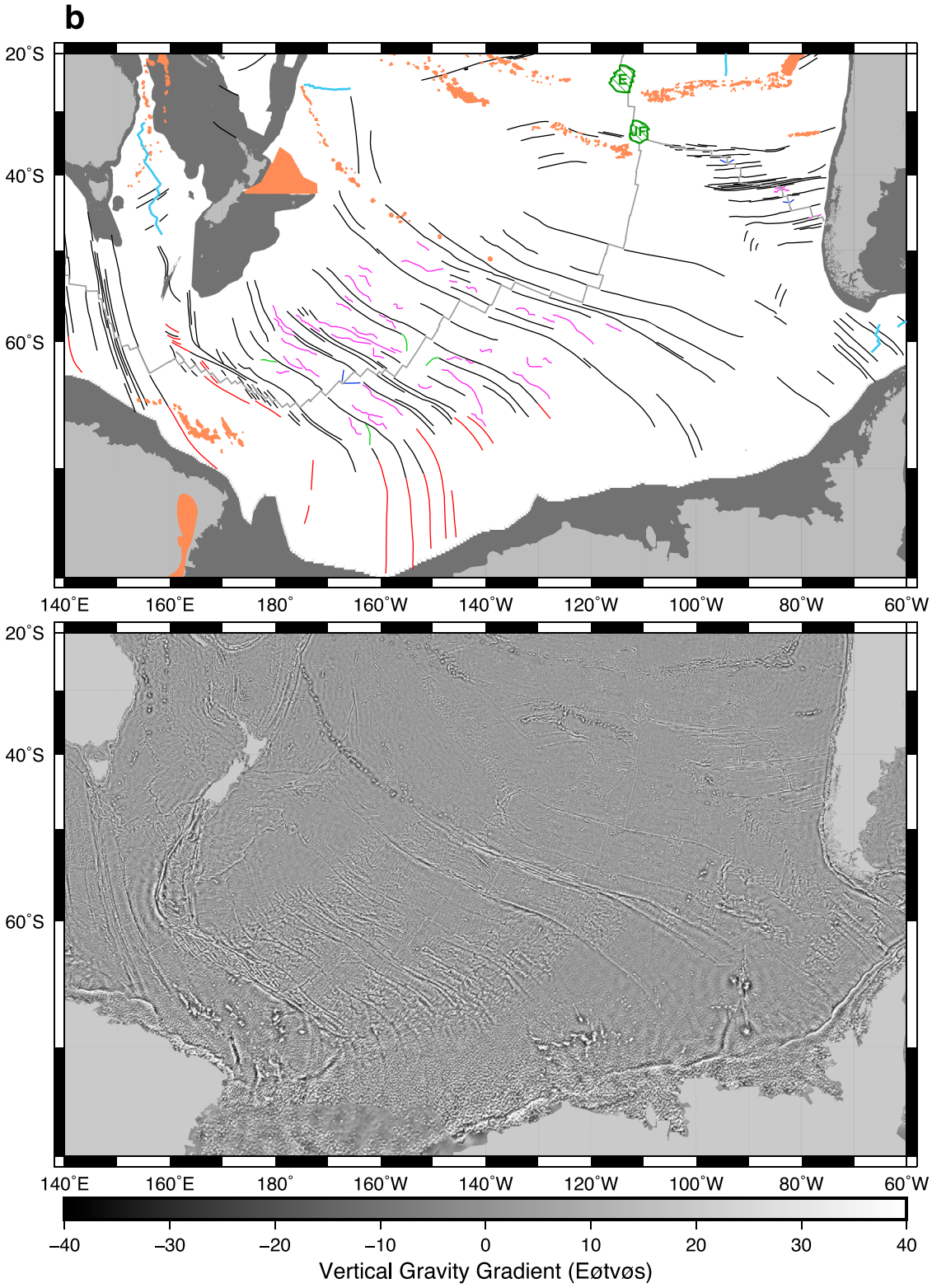

Figure 6. (continued)

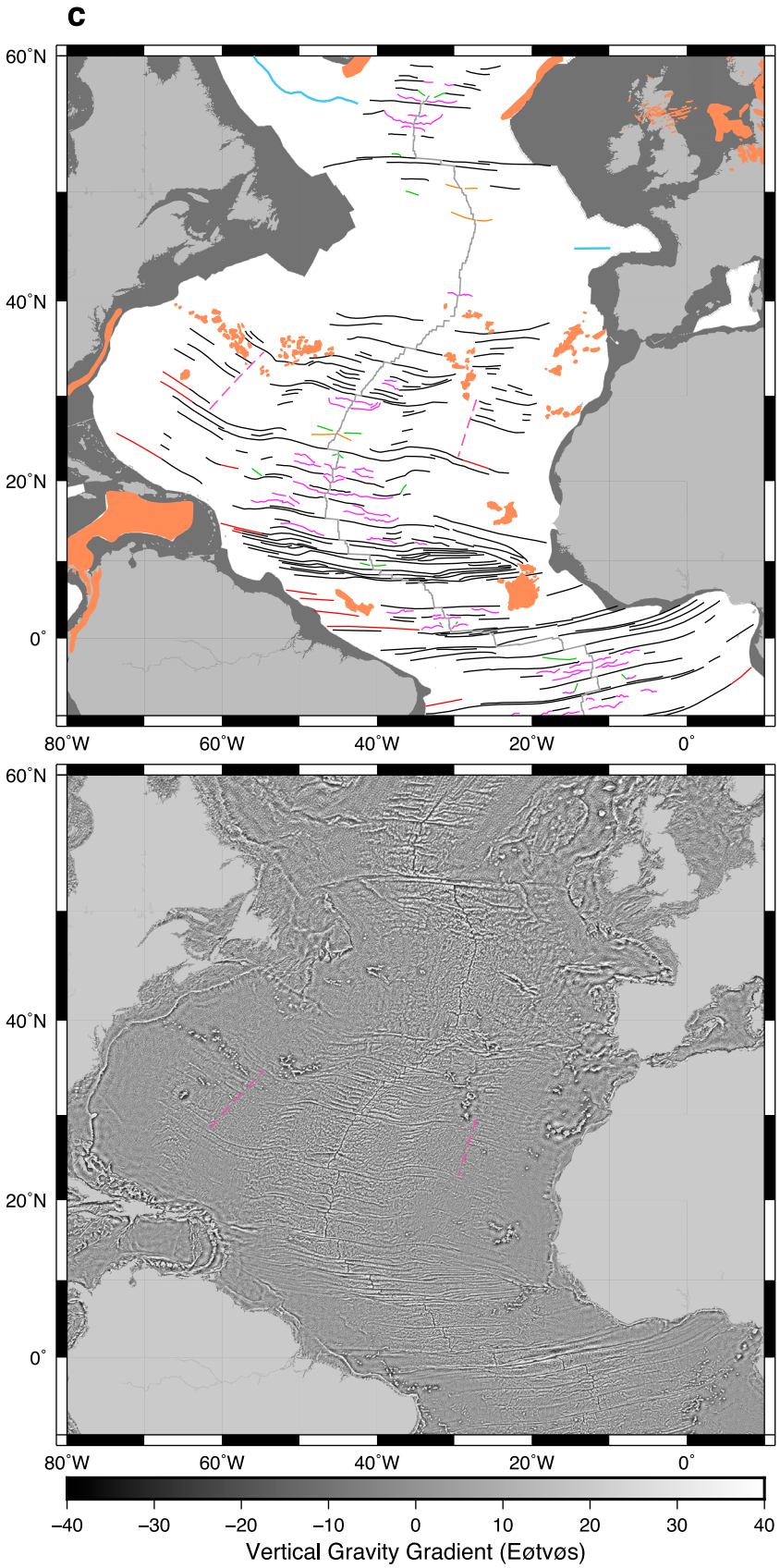

Figure 6. (continued)

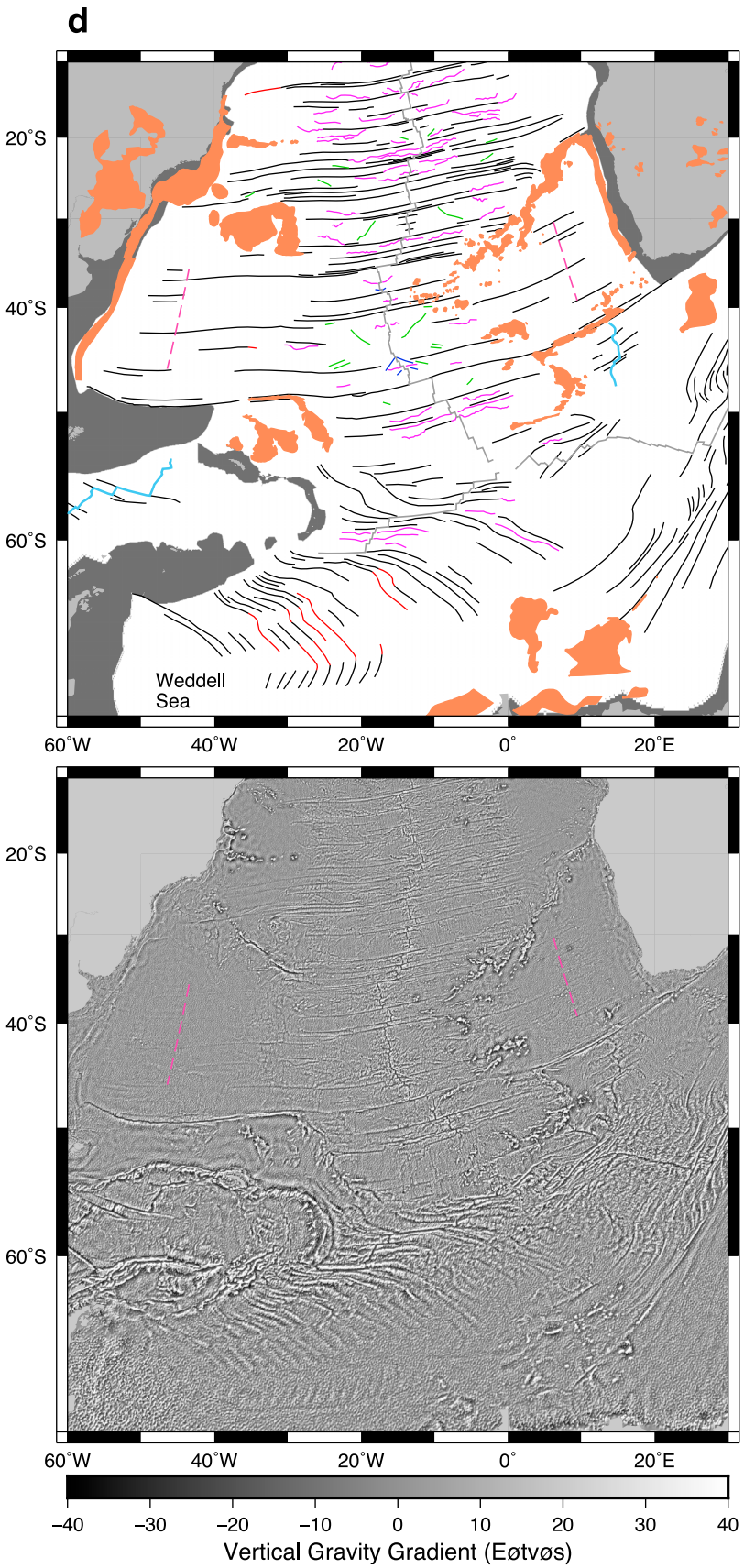

Figure 6. (continued)

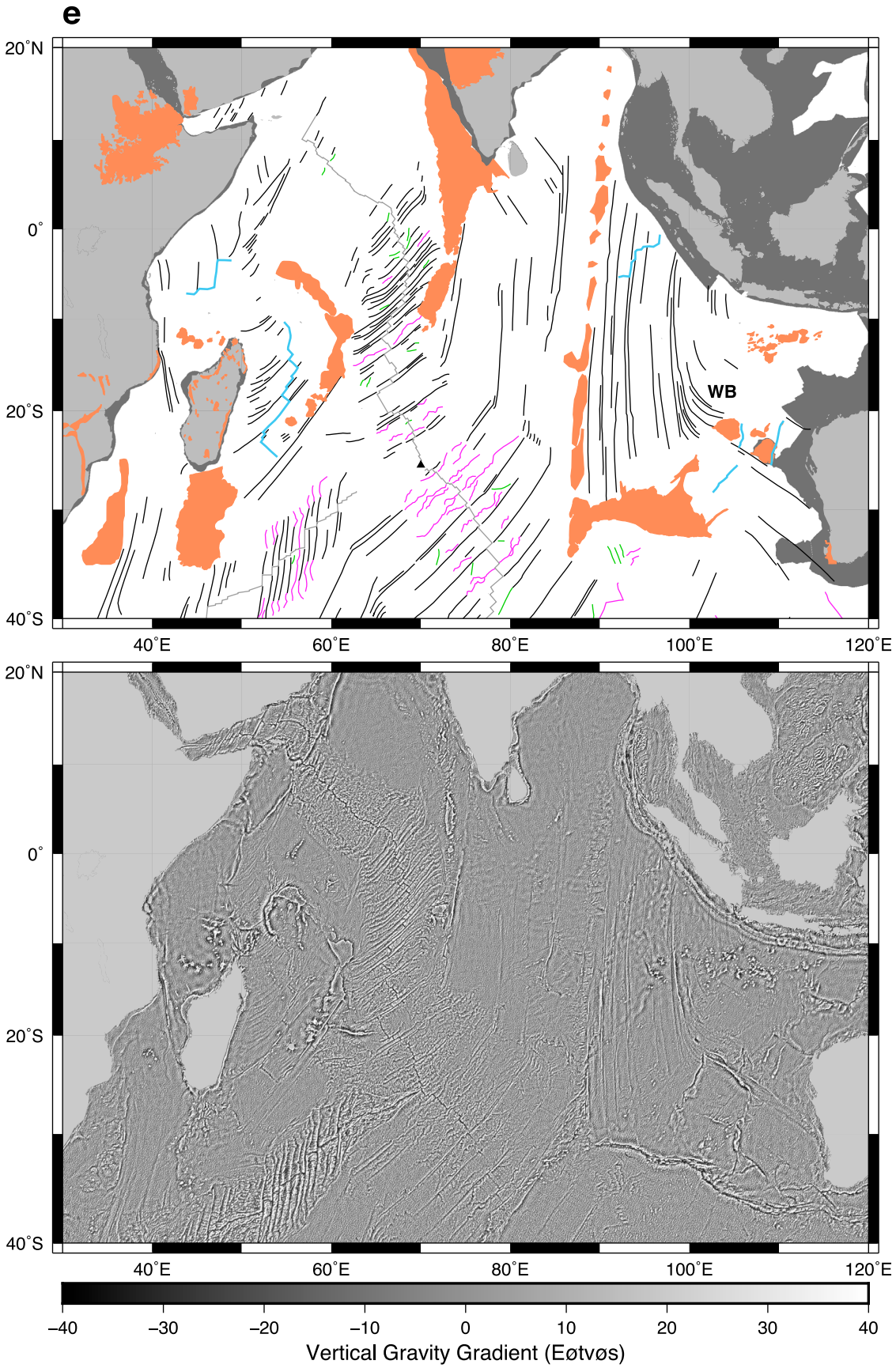

Figure 6. (continued)

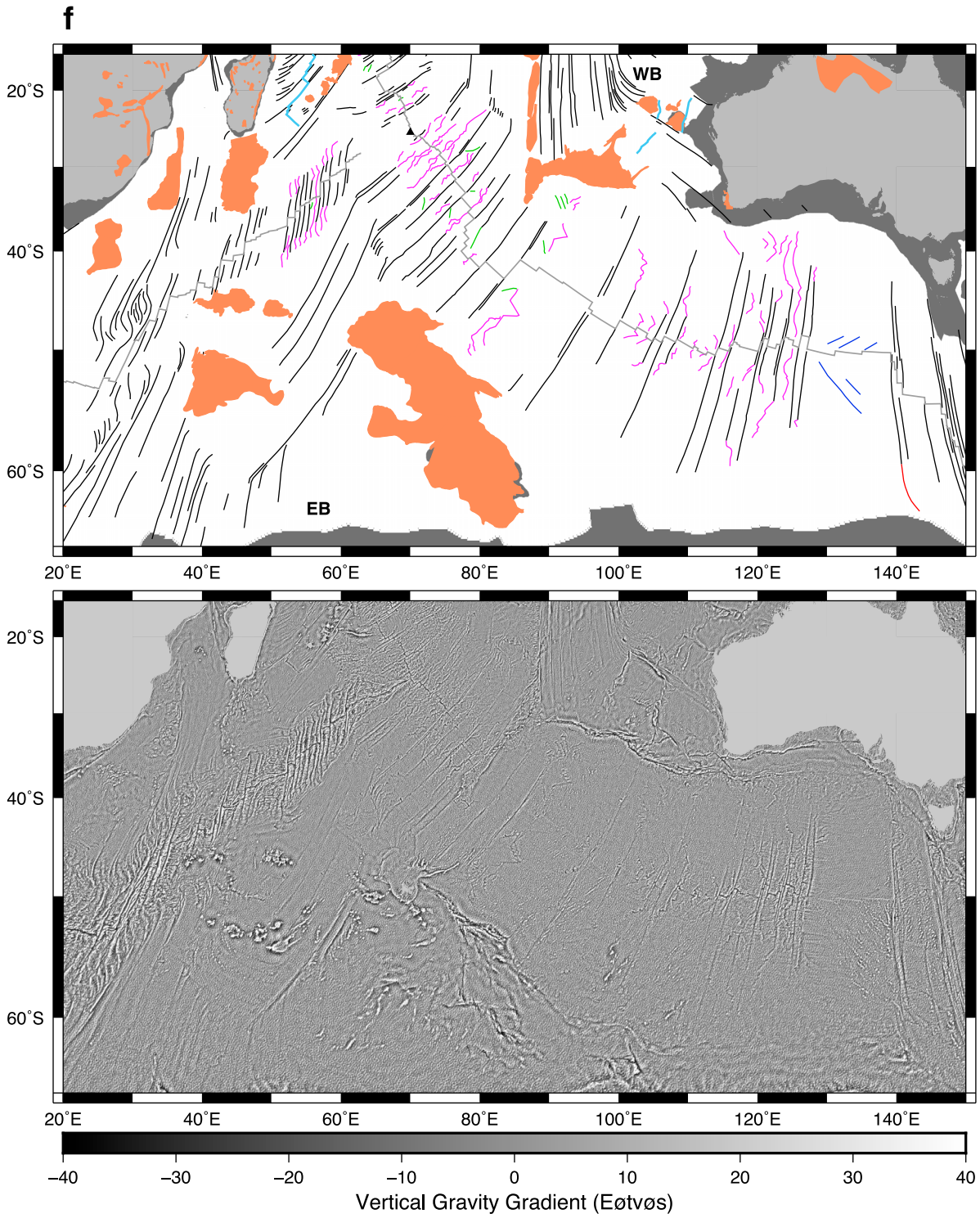

Figure 6. (continued)

more continuous, and can be traced in the gravity data for 100s to >1000 km. Discordant zones that evolve directly from stable FZs (and vice versa) are also more prevalent in these faster slow spreading regimes, and illustrate that stable first-order ridge segmentation is impermanent, even within a long-lived slow spreading regime [*Grindlay et al.*, 1991] (Figure 8).

[38] In regions of ultraslow spreading seafloor morphology is particularly complex. A lack of transform faults and the presence of amagmatic accretionary segments of mid-ocean ridge that may be oblique to the direction of spreading [*Dick et al.*, 2003], inhibit FZ formation. For example, this is the case at the Southwest Indian Ridge between 9°-25°E (Figure 7c), a region of ultraslow spreading identified by

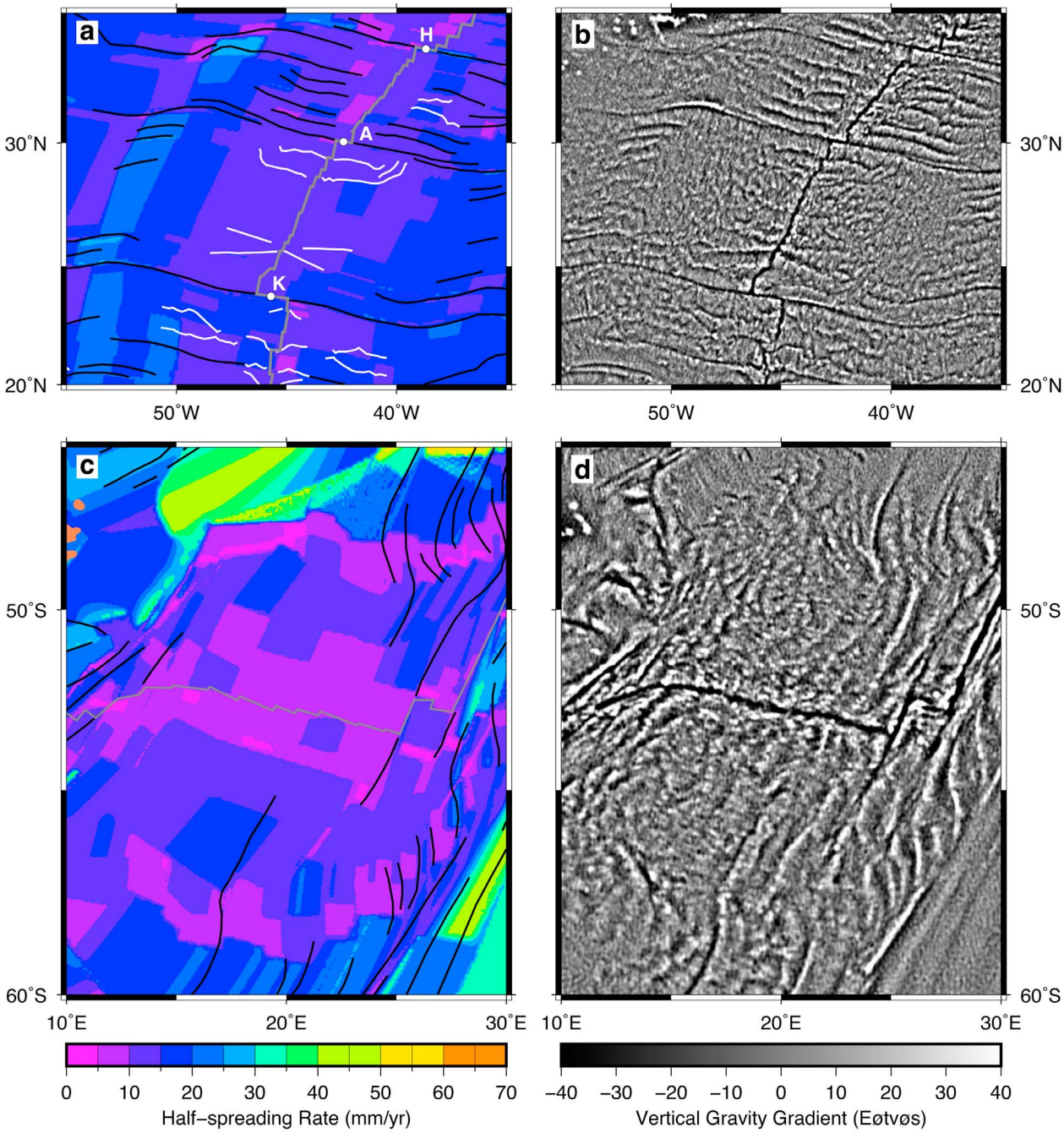

Figure 7. (a, b) Half-spreading rate [*Müller et al.*, 2008] and VGG [*Sandwell and Smith*, 2009] maps for a region of crenulated seafloor between the Kane (K) and Atlantis (A) FZs in the North Atlantic, identified by *Morgan and Parmentier* [1995], and (c, d) a region of ultraslow spreading at the Southwest Indian Ridge identified by *Dick et al.* [2003] between 9 and 25°E. In both of these FZ bounded corridors it is difficult to distinguish well-defined gravity lineations from the VGG maps. FZs are black, and traces of higher-order ridge segmentation are white. H, Hayes FZ. Mid-ocean ridge traces are from *Sandwell and Smith* [2009].

Dick et al. [2003]. Morphological characteristics of ultraslow spreading may also develop in crust that forms at half-spreading rates of up to 10 mm/yr [*Dick et al.*, 2003], which may account for the wide distribution of these rough chaotic regions in slower slow spreading regimes (half-spreading rates up to ~15 mm/yr), and the similarity between the VGG signal for this zone between 9°–25°E and the Kane-Atlantis FZ corridor in the North Atlantic. Additionally, amagmatic accretionary segments are very stable due to the reduced magma supply and lithospheric weakening from dikes [*Dick et al.*, 2003]. For example, there is evidence from the Southwest Indian Ridge that they can exist for >11 Myr

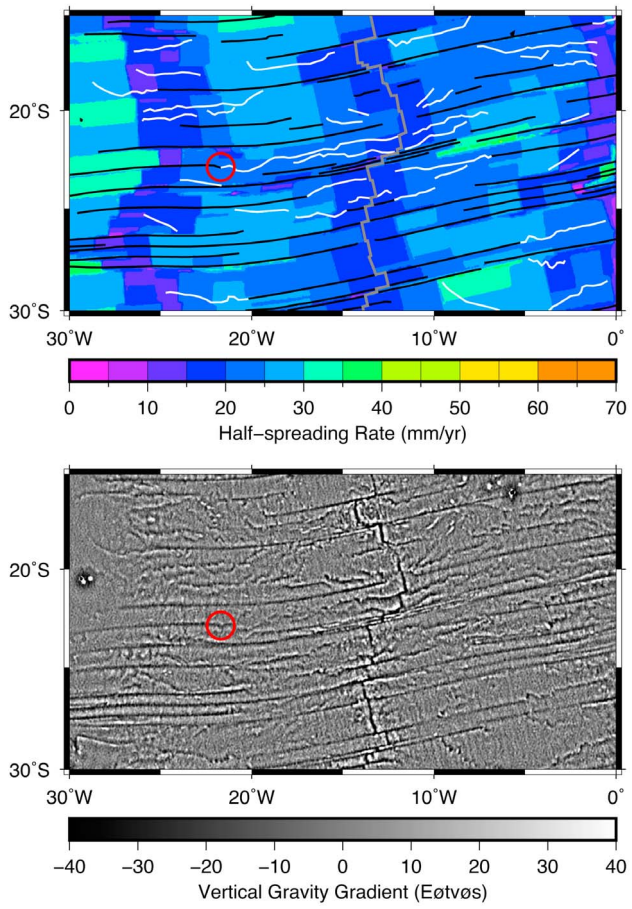

Figure 8. (top) Half-spreading rate [*Müller et al.*, 2008] and (bottom) VGG [*Sandwell and Smith*, 2009] maps for a region of the South Atlantic. Discordant zones form well-defined wavy traces at half-spreading rates of 15–30 mm/yr. An example of discordant zone evolution from a long-lived FZ is highlighted by a red circle. At this time the transform fault from which the stable FZ formed likely became shorter, and therefore less stable. FZs are black, and traces of higher-order ridge segmentation are white. Mid-ocean ridge trace is from *Sandwell and Smith* [2009].

[*Baines et al.*, 2007]. This stability of amagmatic spreading segments may help account for the continual growth of these rough crenulated areas over tens of millions of years despite minor increases or decreases in spreading rate.

5.3. Sedimentation and Volcanism

[39] In the western Pacific FZ traces are sparse and discontinuous (Figure 6a). Seafloor in this region is mid-Cretaceous to Jurassic in age, and has been affected by multiple episodes of seamount and large igneous province emplacement [e.g., *Atwater*, 1989]. The eruption of large igneous provinces has also produced extensive gaps in the Indian Ocean FZ record (Figures 6e and 6f). Thick sediment cover along passive margins also limits our ability to extend FZ traces to continent-ocean boundaries. For example, sediment thickness exceeds 8000 m in the Bay of Bengal southeast of India, and 4000 m along the Atlantic passive margins [*Divins*, 2010]. This is in contrast to the South American active margin, where FZ signals were traced to the trench and sediment thicknesses are between 100 and 500 m [*Divins*, 2010].

5.4. Plate Boundary Reconfiguration Episodes

[40] The appearance and disappearance of FZs can be associated with plate reorganizations [e.g., *Cande et al.*, 1995, 1988], as the reorientation of mid-ocean ridges and/or changes in spreading rate may result in the formation of new or demise of old ridge segments, and hence transform faults from which FZs develop. Additionally, when a mid-ocean ridge becomes reoriented a state of tension or compression develops at the transform fault [*Menard and Atwater*, 1969] that in turn modifies the FZ morphology [e.g., *McCarthy et al.*, 1996] and can produce a bend in its trace that reflects the change in direction of plate motion.

[41] An example of FZ disappearance accompanying a major plate boundary reconfiguration is seen in the central eastern Pacific. Here the Farallon Plate split into the Cocos and Nazca plates at 25 Ma, after which time there was a 5 Myr period of plate readjustment [*Atwater*, 1989]. FZs on the Pacific Plate (e.g., Marquesas FZ) and on the Nazca Plate (e.g., Mendaña FZ - presently being subducted) appear to have stopped forming at this time (Figure 6a). According to *Eakins and Lonsdale* [2003] the reorganization resulted in opening of the transform fault connecting the conjugate Marquesas and Mendaña FZs, initiation of intratransform spreading centers, and the formation of multistrands that are approximately orthogonal to the present-day East Pacific Rise; we were unable to resolve these multistrands in the VGG grids with confidence. Another example of changes in FZ distribution signaling a plate boundary readjustment is seen in the Atlantic. In the North Atlantic several FZ traces on either flank of the mid-Atlantic ridge end synchronously about mid-way through the Cretaceous Normal Superchron; coincidently these terminations are accompanied by a transition from rougher to smoother seafloor (Figure 6c). Both observations provide evidence for an increase in spreading rate. In the South Atlantic we also observe a decrease in the number of FZ traces about mid-way through the Cretaceous Normal Superchron, again suggesting there may have been an increase in spreading rate at this time. For example, on the South American Plate between 35 and 50°S seven FZs were identified on the seafloor that formed during the earlier part of the superchron, while only two of these traces extend to the latter part of the superchron, and additionally another FZ initiates (Figure 6d). A similar pattern exists on the conjugate African Plate.

[42] FZ bends express major spreading-ridge reorientations and are observed in all ocean basins. The more prominent ones in the FZ data set were produced in the Latest Cretaceous, Eocene and roughly mid-way through the Cretaceous Normal Superchron (c. 100 Ma). The latter two suites of FZ bends therefore temporally coincide with a proposed plate reorganization event c. 50 Ma [*Whittaker et al.*, 2007; *Sharp and Clague*, 2006], and potentially with a major swerve of the Pacific Plate 99 Ma [*Veevers*, 2000].

[43] Closely spaced Late Cretaceous and Eocene FZ bends in the North Atlantic, Weddell Sea and southwest Indian Ocean between Antarctica and Africa produce an S-shape in the tectonic fabric of the seafloor (Figures 6c, 6d, and 6f). The older bends reveal a 20° counter-clockwise rotation of

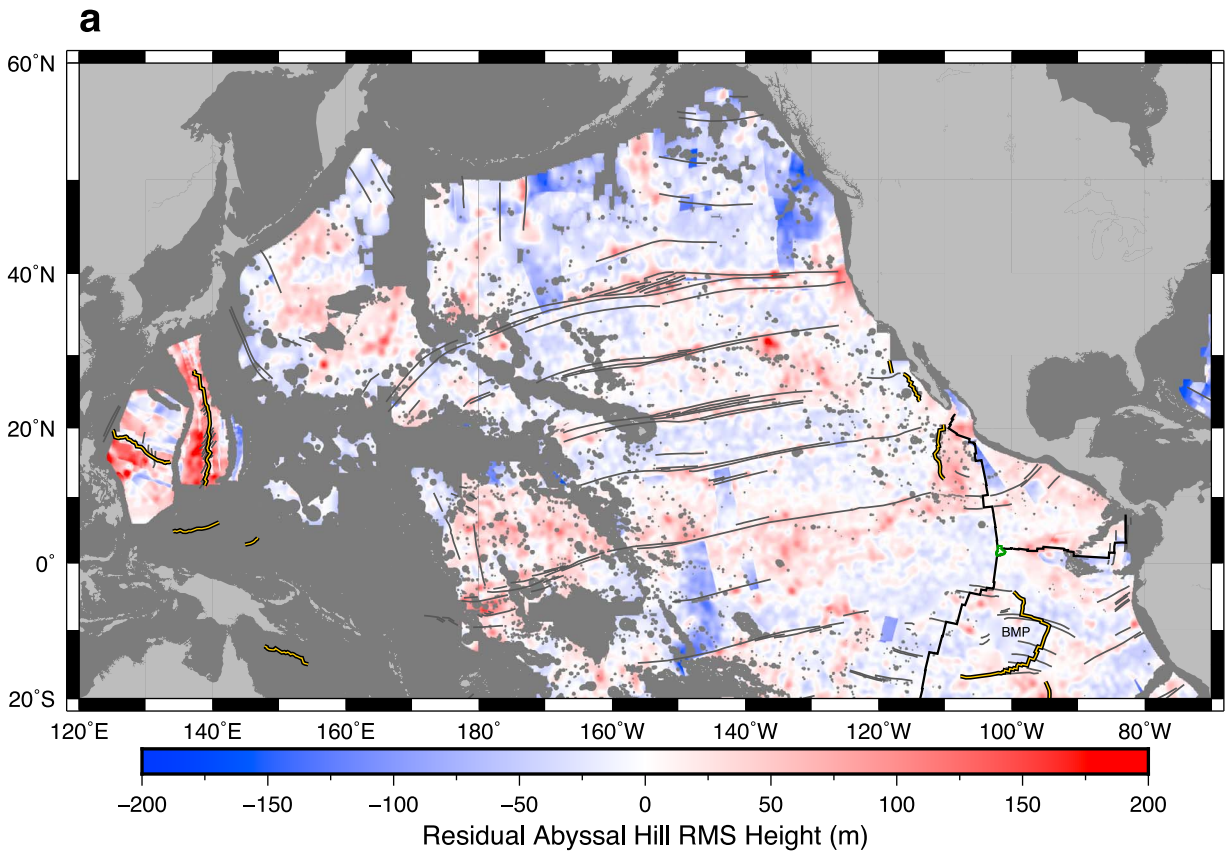

Figure 9. Residual abyssal hill RMS height maps of the ocean basins: (a) North Pacific, (b) South Pacific, (c) North Atlantic, (d) South Atlantic, (e) North Indian, and (f) South Indian. Heights were calculated by removing the effects of spreading rate from the predicted abyssal hill RMS height data of *Goff* [2010]. Regions masked from calculations are dark gray and include continental crust, seamounts, large igneous provinces and regions where sediment thickness exceeds 500 m. FZ traces are dark gray, traces of higher-order ridge segmentation are black, and extinct spreading ridges are yellow on black. Mid-ocean ridge traces are from *Sandwell and Smith* [2009]. In Figure 9a the Galapagos microplate is outlined in green. BMP, Bauer microplate. E, Easter microplate; JF, Juan Fernandez microplate; Mn, Menard FZ (Figure 9b); AR, Agulhas ridge (Figure 9d).

the North America-Africa spreading ridge, a ∼40–45° clockwise rotation of the Antarctica-South America ridge, and a 40–45° counter-clockwise rotation of the Antarctica-Africa ridge [see also *Royer et al.*, 1988], and the younger bends represent the rotation of the spreading ridges back to their original orientation. Along the Mid-Atlantic ridge, south of ∼6°N, FZ traces produce only very broad curvature, indicating only minor changes in spreading direction between South America and Africa.

[44] Three suites of FZ bends from the Indian Ocean and a fourth from the Weddell Sea formed about mid-way through the Cretaceous Normal Superchron. The most prominent and well-preserved FZ bends occur in the Wharton Basin in the eastern Indian Ocean, and resulted from a 50° clockwise reorientation of the Indian-Australian spreading ridge, ∼100 Ma according to *Müller et al.* [1998] (Figure 6e). Conjugate FZ bends in the Enderby Basin and southeast of India (Figures 6e and 6f) indicate a ∼32–38° clockwise change in spreading azimuth at the Indian-Antarctic ridge. Although sea-ice coverage weakens the gravity signal in the circum-Antarctic [*McAdoo and Laxon*, 1997] a fourth set of mid-Cretaceous FZ bends is identifiable in the Weddell Sea (Figure 6d) which expresses a 75° counter-clockwise rotation of the now-subducted Antarctic-South American ridge. There are no major mid-Cretaceous FZ bends in the Atlantic and Pacific ocean basins, if present they must be very broad with only a few degrees change in strike.

6. Data Set Application: Interpreting the Origins of Abyssal Hill Height Anomalies

[45] We have combined our digitized gravity lineations with the computed residual abyssal hill RMS height grid (Figure 9). We have chosen not to analyze the western and central Pacific as most of this domain has been masked out to remove seamounts and large igneous provinces (Figure 9a). The central Pacific has experienced major episodes of volcanism, including one in the Late Cretaceous [*Atwater*, 1989], and separating the effects of intraplate volcanism from true abyssal hill fabric would be a complex task beyond the scope of this investigation.

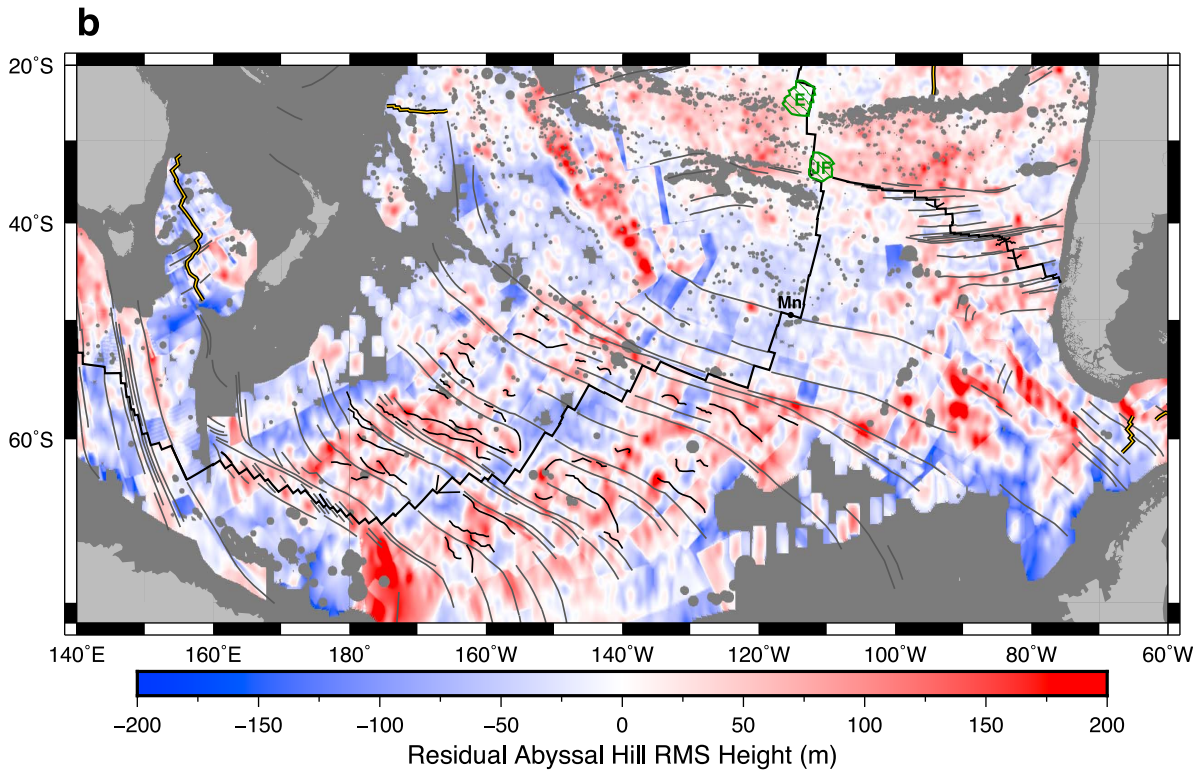

Figure 9. (continued)

6.1. Fracture Zone and Second-Order Discontinuity Fabric

[46] When our gravity lineations data set is combined with the residual abyssal hill RMS height grid it becomes apparent that prominent discordant zone signals remain in the data at several ridges and are associated with positive residual anomalies reaching >100 m. In regions identified previously as "faster slow spreading regimes" (~15–30 mm/year half-rate, Section 5.2) and at the intermediate spreading Southeast Indian Ridge these positive anomalies exactly follow the trace of the wavy discordant zones (Figures 9d and 9f). Highly irregular, wavy traces cover a range of angles relative to the direction of spreading, limiting the success of directional filtering in some areas. Filtering out signals that cover a too wide a range of angles to the direction of spreading would result in removal of the abyssal hill fabric itself [*Goff*, 2010]. Interpretations of abyssal hill RMS height trends in these spreading regimes should consider these remnant second-order discontinuity signals. Additionally, prominent FZ bends and multistrand signals in the Pacific remain in the residual abyssal hill RMS height grids (Figure 9a). Abyssal hill RMS heights in some regions may be almost entirely attributable to spreading rate, with anomalous heights an artifact of remnant discordant zone traces and plate motion changes that alter the azimuth of seafloor spreading lineations, particularly where near-zero residual heights prevail between the traces.

6.2. Pacific Residual Abyssal Hill Height Anomalies

[47] In the northeast and central east Pacific (Figure 9a), abyssal hill RMS heights are generally well predicted by spreading rate; residual anomalies are small (within ±50 m), with a portion of the signal corresponding to the major FZs (as discussed in Section 6.1). There are, however, two prominent linear zones of seafloor in the South Pacific where abyssal hill RMS heights are 50 to >200 m larger than predicted by spreading rate, and FZ traces are absent. Approximately situated between the Easter microplate and the Pacific-Nazca-Antarctic triple junction is a 6000 km east to west trending corridor that crosses the East Pacific Rise (Figures 9b and 10), and on the Pacific Plate west of the Menard FZ there is a 3000 km north-northwest to south-southeast trending feature (Figures 9b and 10).

[48] It is particularly intriguing that such a large positive residual abyssal hill height anomaly should dominate Pacific-Nazca seafloor, considering (1) half-spreading rates at the East Pacific Rise have consistently been very fast, typically exceeding 50 mm/year, and (2) *Whittaker et al.* [2008] found no evidence for anomalously rough or smooth seafloor in this region. We suggest that the observed residual anomaly is produced by palaeomicroplates and remnants of overlapping spreading centers, rather than abyssal hill fabric.

[49] Microplates and overlapping spreading centers dominate the present-day East Pacific Rise, with a notable lack of stable transform faults [*Naar and Hey*, 1989]. This configuration likely prevailed during its evolution [*Eakins and Lonsdale*, 2003; *Searle et al.*, 1995]. Along with the active Galapagos, Easter and Juan Fernandez microplates, the Bauer, Selkirk, Friday and Mendoza palaeo-microplates populate the seafloor. Additionally, *Goff et al.* [1993] identified the Wilkes "nannoplate" (9°S), a smaller unstable microplate-type feature that rotates independently of the

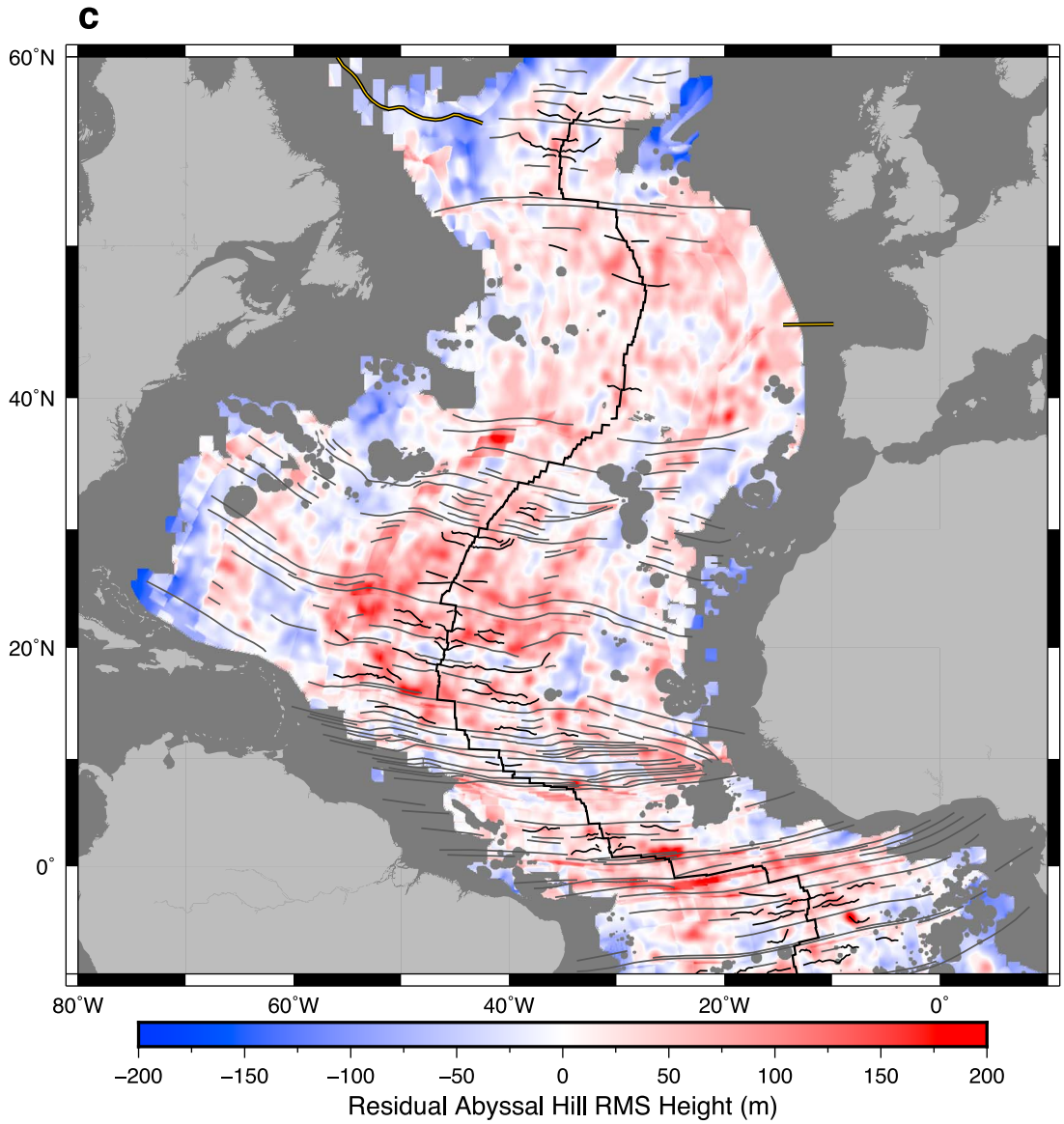

Figure 9. (continued)

adjacent plates; it is likely that these phenomena also existed in the past. *Searle et al.* [1995] pointed out the link between successive microplate formation and very fast spreading at the East Pacific Rise, they noted that between the Easter microplate and the Pacific-Nazca-Antarctic triple junction transform fault slip rates exceed the limit for stable transform faults to exist (145 mm/yr) [*Naar and Hey*, 1989]. This region of high transform slip rates corresponds to the identified ∼east-west residual abyssal hill height anomaly.

[50] We have traced circular patterns in the VGG maps that we suggest may be the signatures of small palaeo-microplates, palaeo-nannoplates or overlapping spreading centers (Figure 10). These features occur adjacent to the Roggeveen Rise, an extinct Pacific-Farallon spreading ridge that was abandoned by a westward ridge jump ∼20 Ma [*Mammerickx et al.*, 1980], and coincide with the largest residual abyssal hill heights within the identified zone. The Roggeveen Rise is the southward continuation of the Mendoza Rise, another Pacific-Farallon spreading ridge that was abandoned by the ∼20 Ma westward ridge jump [*Mammerickx et al.*, 1980]. The residual abyssal hill height anomaly extends north of the Sala Y Gomez ridge between 100 and 88°W, coinciding with the Mendoza Rise. *Searle et al.* [1995] suggested that, since at least chron 6C (∼24 Ma), all seafloor west of the Easter microplate and stretching as far south as the Pacific-Nazca-Antarctic triple junction likely formed at overlapping spreading centers and from microplates. We suggest that this is also the case to the east, and accounts for the observed residual abyssal hill heights across the East Pacific Rise. We find that our palaeo-microplate traces are associated with asymmetric crustal accretion [*Müller et al.*, 2008], which would be expected when microplates become inactive and are transferred to one ridge flank (Figure 11).

[51] The tectonic fabric of the Pacific seafloor largely reflects a spreading rate dependence, however, between the Easter microplate and the Pacific-Nazca-Antarctic triple junction this is not in the typical sense of fast spreading

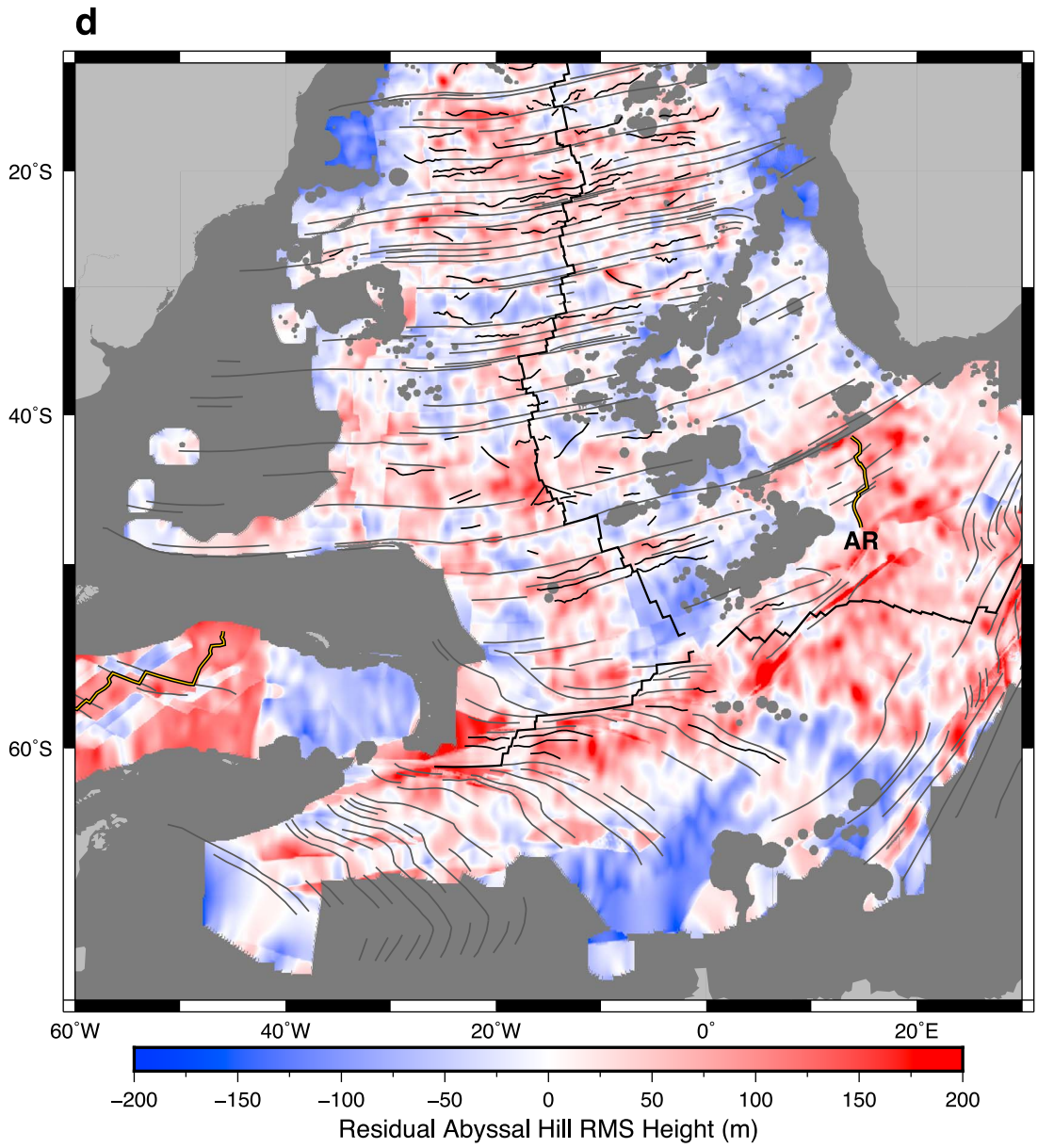

Figure 9. (continued)

producing relatively smooth seafloor [*Menard*, 1967]. In this region we suggest spreading rates have been so high since at least 25 Ma that successive formation of overlapping spreading centers and short-lived microplates has produced chaotic seafloor.

[52] The north-northwest to south-southeast trending anomaly in the southwest Pacific is composed of rough seafloor produced by Late Cretaceous-Early Cenozoic Pacific-Farallon spreading. The southwestern margin of this feature is a triple junction trace [e.g., *Viso et al.*, 2005; *Larson et al.*, 2002; *Cande et al.*, 1982; Seton et al., submitted manuscript, 2011] and separates abyssal hill fabric of different orientations, evident in high-resolution multibeam data [e.g., *Larson et al.*, 2002]. To the east of the boundary abyssal hills trend ~north-south, and to the west abyssal hills trend ~east-west. While it is agreed that the north-south trending abyssal hill fabric originated from Pacific-Farallon spreading, several different models have been proposed concerning the evolution of seafloor to the west of the boundary [*Viso et al.*, 2005; *Larson et al.*, 2002; *Cande et al.*, 1982; Seton et al., submitted manuscript, 2011], that formed during the Cretaceous Normal Superchron, and consequently cannot be dated from magnetic anomaly data.

[53] According to *Viso et al.* [2005] and *Larson et al.* [2002] this boundary traces the southeastward propagation of the Tongareva triple junction that fragmented the Manihiki Plateau ~119 Ma. The Tongareva triple junction comprises the Pacific-Farallon, Farallon-Phoenix and Pacific-Phoenix spreading centers and is named after the Tongareva Atoll [*Larson et al.*, 2002]. In this model the approximately east-west trending abyssal hill fabric formed from north-south oriented Pacific-Phoenix spreading. *Cande et al.* [1982] presented a tectonic history for the southeast Pacific

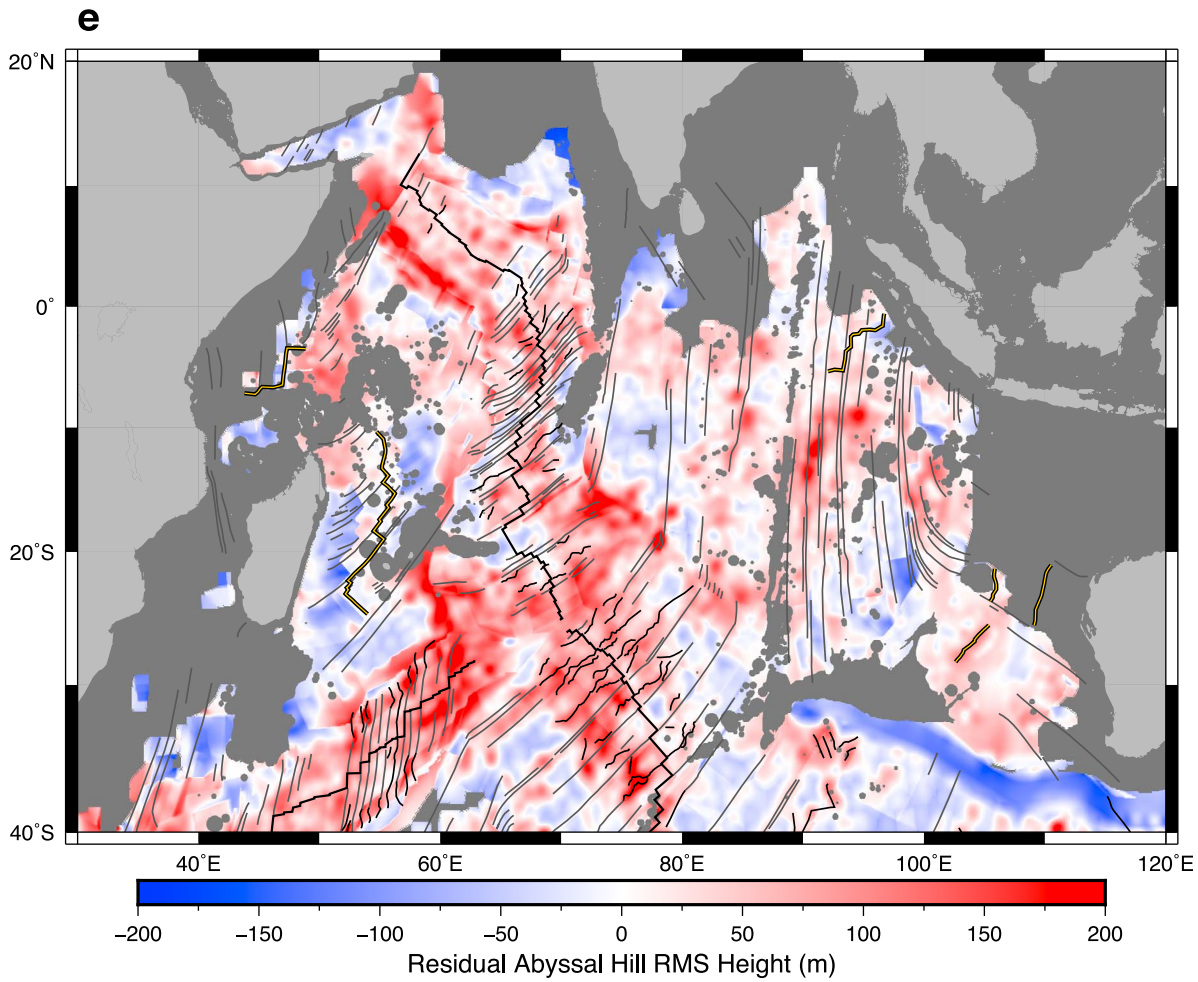

Figure 9. (continued)

based on ship track data. They focused on the Cenozoic evolution of the Pacific-Aluk spreading system and growth of the Antarctic Plate. According to their model, this rough/smooth boundary in the southwest Pacific traces the southeastward migration of the Pacific-Farallon-Aluk triple junction, that was established some time prior to chron 34, and therefore approximately east-west abyssal hills formed at the Pacific-Aluk spreading ridge. In this model the Aluk Plate, and the Antarctic Plate to the west, originated as fragments of the extinct Phoenix Plate. Seton et al. (submitted manuscript, 2011) produced a completely revised plate reconstruction model for the Pacific that incorporates *Taylor*'s [2006] recent findings that the Ontong-Java, Manihiki and Hikurangi plateaus, in the southwest Pacific, formed together as a single massive large igneous province (LIP) 120 Ma, that was subsequently rifted apart. They implemented three triple junctions in their model to fragment this "mega-LIP." The southwest Pacific triple junction trace, according to Seton et al. (submitted manuscript, 2011), records the southeastward migration of the Manihiki-Chasca-Southeast Manihiki triple junction that rifted apart the Manihiki Plateau; the newly proposed Chasca Plate has been completely subducted beneath South America. Therefore east-west trending seafloor fabric to the west of the triple junction trace was produced by Manihiki-Southeast Manihiki spreading, and subsequently by Pacific-Antarctic spreading once the triple junctions shutdown ~86 Ma, coinciding with docking of the Hikurangi Plateau to the Chatham Rise (Seton et al., submitted manuscript, 2011).

[54] The width of the residual RMS anomaly is roughly 300–400 km, suggesting that it formed over ~8–10 Myr according to the half-spreading rates of *Müller et al.* [2008]. Similar residual anomalies are not observed north of 23°N along the Pacific-Farallon ridge, nor further south along the Pacific-Antarctic ridge on seafloor of the same age, indicating that the anomaly is spatially and temporally small in scale. Therefore, this isolated zone of rough seafloor may have been produced by slower spreading rates than were used to compute the residual RMS heights [*Müller et al.*, 2008], rather than by a sub-axial mantle thermal or melt depletion anomaly. In this zone the average abyssal hill RMS heights range from 150 to 250 km [*Goff*, 2010], which according to the relationship between abyssal hill RMS height and half-spreading rate, can be accounted for by a slow half-spreading rate <15–20 mm/yr (Figure 3). *Cande et al.* [1982] identified a fragment of seafloor produced by Pacific-Farallon spreading that became attached to the Antarctic Plate when the Pacific-Antarctic ridge propagated

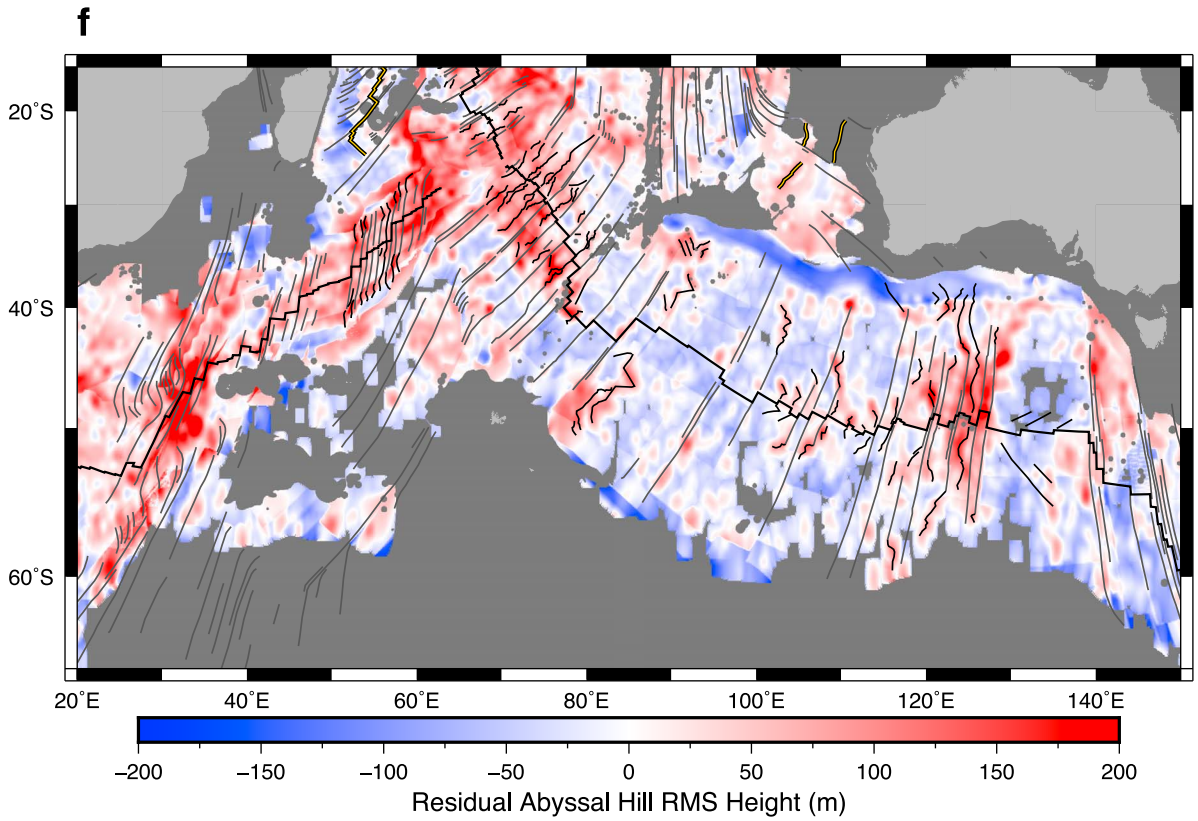

Figure 9. (continued)

north ~50 Ma. This along with the Hudson microplate may, at least partly, account for the positive residual anomaly east of the Hudson Trough.

6.3. Mantle Thermal Anomalies and Mantle Depletion Signatures

[55] Along the Mid-Atlantic, Southwest Indian, Central Indian and Carlsberg ridges residual anomalies produce a broad signal over a wide region, showing little direct correlation with individual discordant zone traces (Figures 9c–9f). This suggests that the residual abyssal hill heights are due to the influence of either anomalous mantle thermal conditions or mantle depletion [*Whittaker et al.*, 2008]. We find that on <70 Ma seafloor in the Central and South Atlantic, and <50 Ma seafloor along the western Indian ridges, positive residual heights dominate, consistent with the Cenozoic seafloor roughness trends determined by *Whittaker et al.* [2008]. As expected this is also the case for seafloor created at the now-extinct Agulhas ridge, southwest of Africa (Figure 9d), where spreading initiated some time during the Cretaceous Normal Superchron and ended at ~61.2 Ma when a westward ridge jump occurred [*Marks and Stock*, 2001].

[56] *Whittaker et al.* [2010] studied the origin of the residual depth anomaly and excessive seafloor roughness at the Australian Antarctic Discordance (~120–128°E). They found that, while 0–83 Ma seafloor is anomalously deep due to the effects of negative dynamic topography and thinned crust near the continental margins, only <20 Ma crust is anomalously rough, resulting from cold and depleted mantle being extracted at the ridge. On >20 Ma seafloor positive residual abyssal hill RMS height anomalies trace the digitized discordant zones, while for crust <20 Ma the positive signal is broad and encompasses the whole domain (Figure 9f). From this we infer that the positive residual signals on crust >20 Ma are likely an artifact of remnant discordant zones, yet <20 Ma abyssal hills are indeed anomalously tall.

7. Conclusions

[57] The tectonic fabric of the seafloor produced at mid-ocean ridges preserves a wealth of information regarding spreading ridge dynamics and the evolution of plate boundaries since 200 Ma. We have used VGG data [*Sandwell and Smith*, 2009] to digitize extinct spreading ridges, FZs and lineations produced by higher-order ridge-segmentation. A new FZ tracking program (P. Wessel et al., manuscript in preparation, 2011) enabled us to quantify the precision of our hand-digitized FZ traces. We tested 20 FZs (10 Atlantic-type and 10 Pacific-type) and in each case the Mean Absolute Deviation from the VGG minima, the signal we aimed to digitize, was less than 3.4 km; less than 1.8 km for the Atlantic-type traces alone. As Pacific-type FZs are delineated by the center of the scarp that separates the trough found in the older crust from the peak observed in the younger crust, we also computed the offset between the hand-digitized Pacific-type FZs and the modeled trace of the maximum slope position. For the 10 Pacific-type FZs

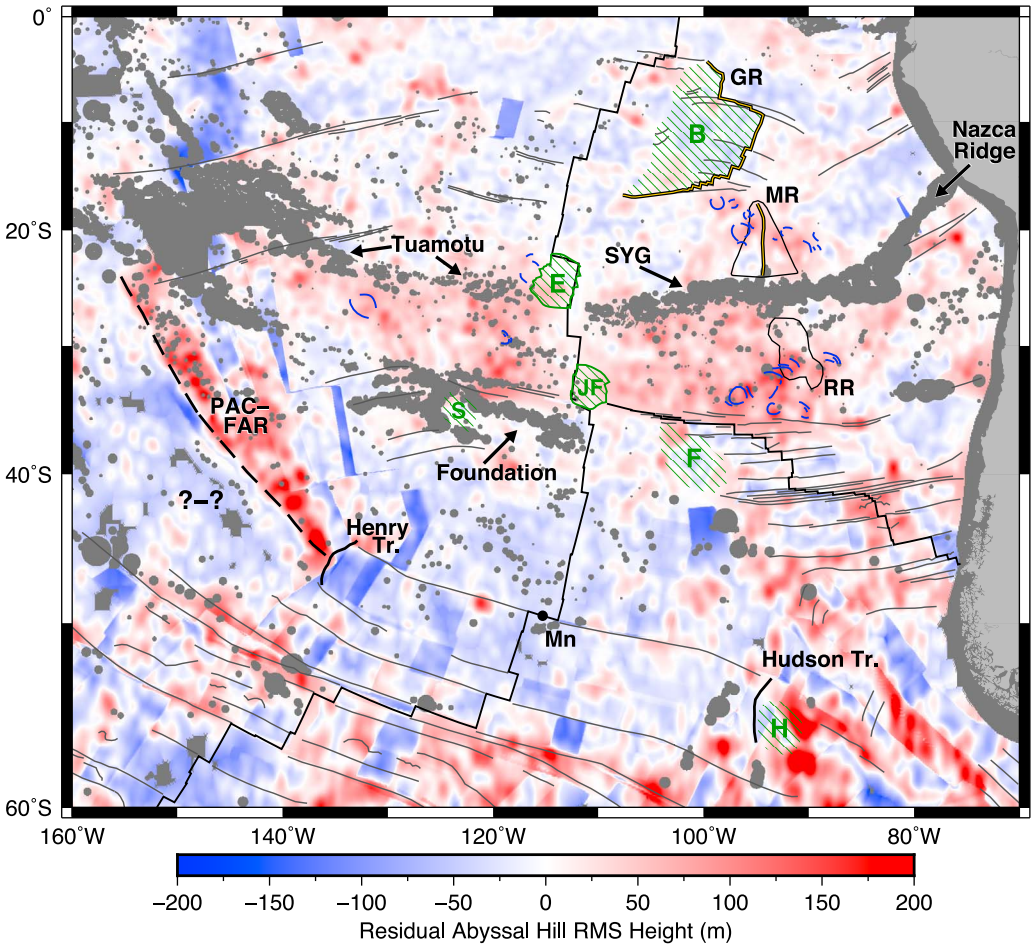

Figure 10. Major tectonic features of the South Pacific, overprinted on residual abyssal hill RMS heights. In the ~east to west trending corridor between the Easter (E) and Juan Fernandez (JF) microplates, and extending north-northwest from Henry Tough, are two linear positive residual abyssal hill height anomalies. Small blue lines trace circular fabric in the seafloor that we suggest may be related to palaeo-microplates or overlapping spreading centers. RR is the outline of the Roggeveen Rise and MR is the Mendoza rise; based on *Mammerickx et al.* [1980] they were traced from the 3600 m and 4100 m ETOPO2v2 [*National Geophysical Data Center*, 2006] bathymetric contours, respectively. The dashed line extending north-northwest from Henry trough is a triple junction trace, to the north of the line the positive residual anomaly corresponds to seafloor produced by Pacific-Farallon spreading (PAC-FAR), and to the south there remains debate as to the spreading configuration (?-?) (see text for discussion of the different plate reconstruction models that have been proposed for the triple junction). FZs and traces of higher-order ridge segmentation are gray and extinct ridges are yellow on black. Mid-ocean ridge trace is from *Sandwell and Smith* [2009]. B, Bauer microplate; Foundation, Foundation Seamounts; F, Friday microplate; GR, Galapagos Ridge; H, Hudson microplate; Mn, Menard FZ; SYG, Sala Y Gomez Ridge; S, Selkirk microplate; Tuamotu, Tuamotu Seamounts.

that we tested the Mean Absolute Deviation was consistently less than 5.4 km. These offsets are small as it must be considered that gravity data only provide an approximation for the underlying base morphology.

[58] Together with the FZs and other gravity lineations, abyssal hills are the other major component of the seafloor tectonic fabric produced at mid-ocean ridges. From the recent abyssal hill RMS height grid of *Goff* [2010] we removed the effects of spreading rate, and combined the resulting residual heights with our digitized data set. Wavy discordant zones produced at half-spreading rates ~15–30 mm/yr (faster slow-spreading regimes), FZ bends and multistrand signatures remain in the abyssal hill data. In regions where residual abyssal hill anomalies do not coincide with lineated gravity anomalies, but form a broad time-dependent signal, anomalous residual heights are likely a function of mantle thermal anomalies or melt-depletion [*Whittaker et al.*, 2008]. There are two prominent near-linear residual anomalies in the South Pacific that we analyzed in detail and attribute to spreading rate controls:

[59] 1. A large swath of seafloor that formed between the Easter microplate and the Pacific-Nazca-Antarctic triple

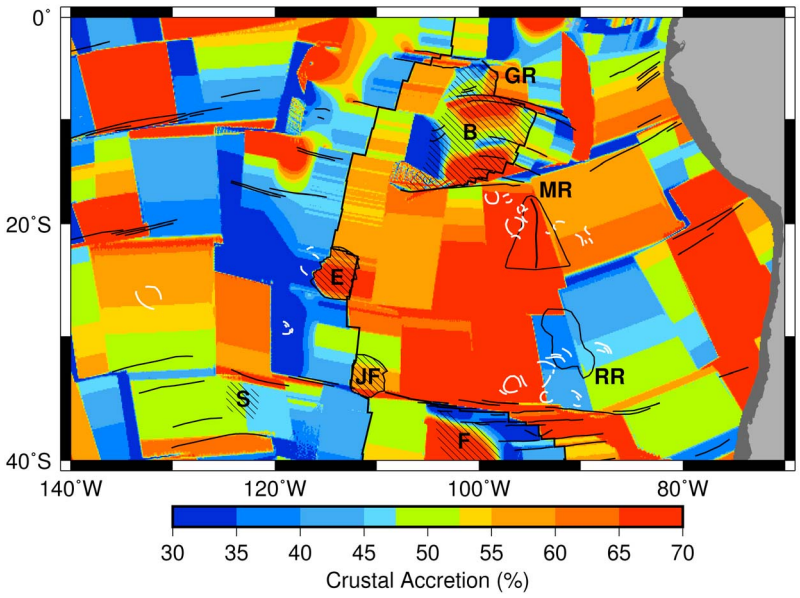

Figure 11. Percentage of crustal accretion on conjugate ridge flanks [*Müller et al.*, 2008]. Here 50% crustal accretion corresponds to symmetric spreading, while smaller and larger values signify asymmetric spreading. White lines are traces of circular fabric in the seafloor that we suggest may be related to palaeo-microplates or overlapping spreading centers, and correspond to zones of positive and negative crustal accretion (reds and blues). See Figure 10 for details of other tectonic fabric traces.

junction, and extending north between the Sala Y Gomez ridge and the Bauer microplate, comprises chaotic tectonic fabric including the traces of palaeo-microplates and remnants of overlapping spreading centers. Seafloor half-spreading rates were so fast during its formation, as much as >70 mm/yr, that a stable plate boundary configuration including transform faults appears to have been absent [see also *Searle et al.*, 1995]. It is likely that these features dominate the gravity signal and therefore the data do not isolate abyssal hill heights.

[60] 2. We consider it unlikely that a prominent 3000 km long north-northwest to south-southeast trending anomaly in the southeast region of the Pacific Plate, produced by Pacific-Farallon spreading, resulted from melt depletion or a mantle thermal anomaly. There are no proximal hot spots during formation, and it has a limited spatial and temporal extent. Additionally, as abyssal hill heights in this zone cover the range attributed to half-spreading rates <15–20 mm/yr, we therefore assume that Pacific-Farallon spreading was much slower than predicted by *Müller et al.* [2008] during formation; demonstrating the seafloor tectonic fabric trends enable existing plate motion models to be better constrained.

[61] **Acknowledgments.** We thank John Goff for making his abyssal hill RMS height grid available to us. Figures 2–11 were produced using GMT v4.5.7 [*Wessel and Smith*, 1998]. Our tectonic fabric traces and the residual abyssal hill RMS height grid are available in several different file formats through the AuScope EarthByte FTP site: ftp.earthbyte.org/earthbyte/Seafloor_Tectonic_Fabric. The original data set is also stored in a continually maintained database, hosted by The Global Seafloor Fabric and Magnetic Lineation Data Base Project Web site: http://www.soest.hawaii.edu/PT/GSFML/. This will enable the data set to evolve in the future by incorporating additions and modifications. K.J.M. was supported by ARC grant DP0986377, R.D.M. was supported by ARC grant FL0992245 and NSF grant OCE-0752543, P.W. was supported by NSF grant OCE-0752543, and J.M.W. was supported by a Statoil research grant. We thank Rupert Sutherland and an anonymous reviewer for their constructive comments that improved the quality of the manuscript.

References

Andersen, O. B., P. Knudsen, and P. A. M. Berry (2010), The DNSC08GRA global marine gravity field from double retracked satellite altimetry, *J. Geod.*, *84*(3), 191–199, doi:10.1007/s00190-009-0355-9.

Atwater, T. (1989), Plate tectonic history of the northeast Pacific and western North America, in *The Geology of North America*, edited by E. L. Winterer, D. M. Hussong, and R. W. Decker, pp. 21–72, Geol. Soc. of Am., Boulder, Colo.

Baines, A. G., M. J. Cheadle, H. J. B. Dick, A. H. Scheirer, B. E. John, N. J. Kusznir, and T. Matsumoto (2007), Evolution of the Southwest Indian Ridge from 55°45′E to 62°E: Changes in plate-boundary geometry since 26 Ma, *Geochem. Geophys. Geosyst.*, *8*, Q06022, doi:10.1029/2006GC001559.

Briais, A., and M. Rabinowicz (2002), Temporal variations of the segmentation of slow to intermediate spreading mid-ocean ridges: 1. Synoptic observations based on satellite altimetry data, *J. Geophys. Res.*, *107*(B5), 2098, doi:10.1029/2001JB000533.

Cande, S. C., E. M. Herron, and B. R. Hall (1982), The early Cenozoic tectonic history of the southeast Pacific, *Earth Planet. Sci. Lett.*, *57*(1), 63–74, doi:10.1016/0012-821X(82)90173-X.

Cande, S. C., J. L. LaBrecque, and W. F. Haxby (1988), Plate kinematics of the South Atlantic: Chron C34 to present, *J. Geophys. Res.*, *93*(B11), 13,479–13,492, doi:10.1029/JB093iB11p13479.

Cande, S. C., C. A. Raymond, J. Stock, and W. F. Haxby (1995), Geophysics of the Pitman Fracture Zone and Pacific-Antarctic plate motions during the Cenozoic, *Science*, *270*(5238), 947–953, doi:10.1126/science.270.5238.947.

Chen, Y., and W. J. Morgan (1990), A nonlinear rheology model for mid-ocean ridge axis topography, *J. Geophys. Res.*, *95*(B11), 17,583–17,604, doi:10.1029/JB095iB11p17583.

Coffin, M. F., and O. Eldholm (1994), Large igneous provinces: Crustal structure, dimensions, and external consequences, *Rev. Geophys.*, *32*(1), 1–36, doi:10.1029/93RG02508.

Collette, B. J. (1974), Thermal contraction joints in a spreading seafloor as origin of fracture zones, *Nature*, *251*(5473), 299–300, doi:10.1038/251299a0.

Collette, B. J. (1986), Fracture zones in the North Atlantic: Morphology and a model, *J. Geol. Soc.*, *143*(5), 763–774, doi:10.1144/gsjgs.143.5.0763.

De Alteriis, G., L. Gilg Capar, and J. L. Olivet (1998), Matching satellite derived gravity signatures and seismicity patterns along mid-ocean ridges, *Terra Nova*, *10*(4), 177–182, doi:10.1046/j.1365-3121.1998.00190.x.

DeMets, C., R. G. Gordon, and D. F. Argus (2010), Geologically current plate motions, *Geophys. J. Int.*, *181*(1), 1–80, doi:10.1111/j.1365-246X.2009.04491.x.

Dick, H. J. B., J. Lin, and H. Schouten (2003), An ultraslow-spreading class of ocean ridge, *Nature*, *426*(6965), 405–412, doi:10.1038/nature02128.

Divins, D. L. (2010), NGDC total sediment thickness of the world's oceans and marginal seas, 9 October 2010, http://www.ngdc.noaa.gov/mgg/sedthick/sedthick.html, Natl. Geophys. Data Cent., Boulder, Colo.

Eakins, B. W., and P. F. Lonsdale (2003), Structural patterns and tectonic history of the Bauer microplate, eastern tropical Pacific, *Mar. Geophys. Res.*, *24*(3–4), 171–205, doi:10.1007/s11001-004-5882-4.

Fox, P. J., and D. G. Gallo (1986), The geology of the North Atlantic transform plate boundaries and their aseismic extensions, in *The Geology of North America, The Western North Atlantic Region*, edited by P. R. Vogt and B. E. Tucholke, pp. 157–172, Geol. Soc. of Am., Boulder, Colo.

Fox, P. J., N. R. Grindlay, and K. C. MacDonald (1991), The Mid-Atlantic Ridge (31°S-34°30′S): Temporal and spatial variations of accretionary processes, *Mar. Geophys. Res.*, *13*(1), 1–20, doi:10.1007/BF02428193.

Gahagan, L. M., C. R. Scotese, J.-Y. Royer, D. T. Sandwell, J. K. Winn, R. L. Tomlins, M. I. Ross, J. S. Newman, R. D. Müller, and C. L. Mayes (1988), Tectonic fabric map of the ocean basins from satellite altimetry data, *Tectonophysics*, *155*(1–4), 1–6, 11–26, doi:10.1016/0040-1951(88)90258-2.

Goff, J. A. (2010), Global prediction of abyssal hill root-mean-square heights from small-scale altimetric gravity variability, *J. Geophys. Res.*, *115*, B12104, doi:10.1029/2010JB007867.

Goff, J. A., D. J. Fornari, J. R. Cochran, C. Keeley, and A. Malinverno (1993), Wilkes transform system and "nannoplate," *Geology*, *21*(7), 623–626, doi:10.1130/0091-7613(1993)021<0623:WTSAN>2.3.CO;2.

Goff, J. A., Y. Ma, A. Shah, J. R. Cochran, and J.-C. Sempéré (1997), Stochastic analysis of seafloor morphology on the flank of the Southeast Indian Ridge: The influence of ridge morphology on the formation of abyssal hills, *J. Geophys. Res.*, *102*(B7), 15,521–15,534, doi:10.1029/97JB00781.

Grindlay, N. R., P. J. Fox, and K. C. Macdonald (1991), Second-order ridge axis discontinuities in the south Atlantic: Morphology, structure, and evolution, *Mar. Geophys. Res.*, *13*, 21–49, doi:10.1007/BF02428194.

Hey, R. N. (1977), A new class of "pseudofaults" and their bearing on plate tectonics: A propagating rift model, *Earth Planet. Sci. Lett.*, *37*(2), 321–325, doi:10.1016/0012-821X(77)90177-7.

Hey, R. N., F. K. Duennebier, and W. J. Morgan (1980), Propagating rifts on mid-ocean ridges, *J. Geophys. Res.*, *85*(B7), 3647–3658, doi:10.1029/JB085iB07p03647.

Katz, R. F., R. Ragnarsson, and E. Bodenschatz (2005), Tectonic microplates in a wax model of sea-floor spreading, *N. J. Phys.*, *7*, 37, doi:10.1088/1367-2630/7/1/037.

Kruse, S. E., M. C. McCarthy, M. R. Brudzinski, and M. E. Ranieri (1996), Evolution and strength of Pacific fracture zones, *J. Geophys. Res.*, *101*(B6), 13,731–13,740, doi:10.1029/96JB00645.

Larson, R. L., R. A. Pockalny, R. F. Viso, E. Erba, L. J. Abrams, B. P. Luyendyk, J. M. Stock, and R. W. Clayton (2002), Mid-Cretaceous tectonic evolution of the Tongareva triple junction in the southwestern Pacific Basin, *Geology*, *30*(1), 67–70, doi:10.1130/0091-7613(2002)030<0067:MCTEOT>2.0.CO;2.

Lonsdale, P. (1989), Segmentation of the Pacific-Nazca spreading center, 1°N-20°S, *J. Geophys. Res.*, *94*(B9), 12,197–12,225.

MacDonald, K. C., R. M. Haymon, S. P. Miller, J. C. Sempéré, and P. J. Fox (1988), Deep-tow and SeaBeam studies of dueling propagating ridges on the East Pacific Rise near 20 40 S, *J. Geophys. Res.*, *93*(B4), 2875–2898, doi:10.1029/JB093iB04p02875.

MacDonald, K. C., D. S. Scheirer, and S. M. Carbotte (1991), Mid-ocean ridges: Discontinuities, segments and giant cracks, *Science*, *253*(5023), 986–994, doi:10.1126/science.253.5023.986.

Malinverno, A. (1991), Inverse square-root dependence of mid-ocean-ridge flank roughness on spreading rate, *Nature*, *352*(6330), 58–60, doi:10.1038/352058a0.

Mammerickx, J., E. Herron, and L. Dorman (1980), Evidence for two fossil spreading ridges in the southeast Pacific, *Geol. Soc. Am. Bull*, *91*(5), 263–271.

Marks, K., and J. Stock (2001), Evolution of the Malvinas plate south of Africa, *Mar. Geophys. Res.*, *22*(4), 289–302, doi:10.1023/A:1014638325616.

McAdoo, D., and S. Laxon (1997), Antarctic tectonics: Constraints from an ERS-1 satellite marine gravity field, *Science*, *276*(5312), 556–561, doi:10.1126/science.276.5312.556.

McCarthy, M. C., S. E. Kruse, M. R. Brudzinski, and M. E. Ranieri (1996), Changes in plate motions and the shape of Pacific fracture zones, *J. Geophys. Res.*, *101*(B6), 13,715–13,730, doi:10.1029/96JB00646.

Menard, H. W. (1967), Sea floor spreading, topography, and the second layer, *Science*, *157*(3791), 923–924, doi:10.1126/science.157.3791.923.

Menard, H. W., and T. Atwater (1969), Origin of fracture zone topography, *Nature*, *222*(5198), 1037–1040, doi:10.1038/2221037a0.

Michaud, F., et al. (2006), Oceanic-ridge subduction vs. slab break off: Plate tectonic evolution along the Baja California Sur continental margin since 15 Ma, *Geology*, *34*(1), 13, doi:10.1130/g22050.1.

Mihut, D., and R. D. Müller (1998), Volcanic margin formation and Mesozoic rift propagators in the Cuvier Abyssal Plain off Western Australia, *J. Geophys. Res.*, *103*(B11), 27,135–27,149, doi:10.1029/97JB02672.

Miller, H. G., and V. Singh (1994), Potential field tilt-a new concept for location of potential field sources, *J. Appl. Geophys.*, *32*(2–3), 213–217, doi:10.1016/0926-9851(94)90022-1.

Morgan, J. P., and Y. J. Chen (1993a), The genesis of oceanic crust: Magma injection, hydrothermal circulation, and crustal flow, *J. Geophys. Res.*, *98*(B4), 6283–6297, doi:10.1029/92JB02650.

Morgan, J. P., and Y. J. Chen (1993b), Dependence of ridge-axis morphology on magma supply and spreading rate, *Nature*, *364*(6439), 706–708, doi:10.1038/364706a0.

Morgan, J. P., and E. M. Parmentier (1985), Causes and rate-limiting mechanisms of ridge propagation: A fracture mechanics model, *J. Geophys. Res.*, *90*(B10), 8603–8612, doi:10.1029/JB090iB10p08603.

Morgan, J. P., and E. M. Parmentier (1995), Crenulated seafloor: Evidence for spreading-rate dependent structure of mantle upwelling and melting beneath a mid-oceanic spreading center, *Earth Planet. Sci. Lett.*, *129*(1–4), 73–84, doi:10.1016/0012-821X(94)00227-P.

Morgan, J. P., and D. T. Sandwell (1994), Systematics of ridge propagation south of 30°S, *Earth Planet. Sci. Lett.*, *121*(1–2), 245–258, doi:10.1016/0012-821X(94)90043-4.

Müller, R. D., and W. R. Roest (1992), Fracture zones in the North Atlantic from combined Geosat and Seasat data, *J. Geophys. Res.*, *97*(B3), 3337–3350, doi:10.1029/91JB02605.

Müller, R. D., D. T. Sandwell, B. E. Tucholke, J. G. Sclater, and P. R. Shaw (1991), Depth to basement and geoid expression of the Kane Fracture Zone: A comparison, *Mar. Geophys. Res.*, *13*(2), 105–129.

Müller, R. D., D. Mihut, and S. Baldwin (1998), A new kinematic model for the formation and evolution of the west and northwest Australian margin, in *The Sedimentary Basins of Western Australia 2*, edited by P. G. Purcell and R. R. Purcell, pp. 55–72, Pet. Explor. Soc. of Aust., Perth, West. Aust.

Müller, R. D., M. Sdrolias, C. Gaina, and W. R. Roest (2008), Age, spreading rates, and spreading asymmetry of the world's ocean crust, *Geochem. Geophys. Geosyst.*, *9*, Q04006, doi:10.1029/2007GC001743.

Naar, D. F., and R. N. Hey (1989), Speed limit for oceanic transform faults, *Geology*, *17*(5), 420–422, doi:10.1130/0091-7613(1989)017<0420:SLFOTF>2.3.CO;2.

National Geophysical Data Center (2006), ETOPO2v2 global gridded 2-minute database, http://www.ngdc.noaa.gov/mgg/global/etopo2.html, Boulder, Colo.

Parmentier, E. M., and W. F. Haxby (1986), Thermal stresses in the oceanic lithosphere: Evidence from geoid anomalies at fracture zones, *J. Geophys. Res.*, *91*(B7), 7193–7204, doi:10.1029/JB091iB07p07193.

Royer, J.-Y., P. Patriat, H. W. Bergh, and C. R. Scotese (1988), Evolution of the Southwest Indian Ridge from the Late Cretaceous (anomaly 34) to the Middle Eocene (anomaly 20), *Tectonophysics*, *155*(1–4), 235–260, doi:10.1016/0040-1951(88)90268-5.

Ryan, W. B. F., et al. (2009), Global Multi-Resolution Topography synthesis, *Geochem. Geophys. Geosyst.*, *10*, Q03014, doi:10.1029/2008GC002332.

Sandwell, D. T. (1984), Thermomechanical evolution of oceanic fracture zones, *J. Geophys. Res.*, *89*(B13), 11,401–11,413, doi:10.1029/JB089iB13p11401.

Sandwell, D. T., and G. Schubert (1982), Lithospheric flexure at fracture zones, *J. Geophys. Res.*, *87*(B6), 4657–4667.

Sandwell, D. T., and W. H. F. Smith (1997), Marine gravity anomaly from Geosat and ERS 1 satellite altimetry, *J. Geophys. Res.*, *102*(B5), 10,039–10,054, doi:10.1029/96JB03223.

Sandwell, D. T., and W. H. F. Smith (2005), Retracking ERS-1 altimeter waveforms for optimal gravity field recovery, *Geophys. J. Int.*, *163*(1), 79–89, doi:10.1111/j.1365-246X.2005.02724.x.

Sandwell, D. T., and W. H. F. Smith (2009), Global marine gravity from retracked Geosat and ERS-1 altimetry: Ridge segmentation versus spreading rate, *J. Geophys. Res.*, *114*, B01411, doi:10.1029/2008JB006008.

Schouten, H., H. J. B. Dick, and K. D. Klitgord (1987), Migration of mid-ocean-ridge volcanic segments, *Nature*, *326*(6116), 835–839, doi:10.1038/326835a0.

Searle, R. C., J. Francheteau, and B. Cornaglia (1995), New observations on mid-plate volcanism and the tectonic history of the Pacific plate, Tahiti to Easter microplate, *Earth Planet. Sci. Lett.*, *131*(3–4), 395–421, doi:10.1016/0012-821X(95)00018-8.

Sempéré, J. C., J. Lin, H. S. Brown, H. Schouten, and G. Purdy (1993), Segmentation and morphotectonic variations along a slow-spreading center: The Mid-Atlantic Ridge (24 00′N-30 40′N), *Mar. Geophys. Res.*, *15*(3), 153–200, doi:10.1007/BF01204232.

Sharp, W. D., and D. A. Clague (2006), 50-Ma initiation of Hawaiian-Emperor bend records major change in Pacific plate motion, *Science*, *313*(5791), 1281–1284, doi:10.1126/science.1128489.

Sibuet, J. C., S. P. Srivastava, and W. Spakman (2004), Pyrenean orogeny and plate kinematics, *J. Geophys. Res.*, *109*, B08104, doi:10.1029/2003JB002514.

Small, C., and D. T. Sandwell (1992), An analysis of ridge axis gravity roughness and spreading rate, *J. Geophys. Res.*, *97*(B3), 3235–3245, doi:10.1029/91JB02465.

Small, C., and D. T. Sandwell (1994), Imaging mid-ocean ridge transitions with satellite gravity, *Geology*, *22*(2), 123–126, doi:10.1130/0091-7613(1994)022<0123:IMORTW>2.3.CO;2.

Smith, W. H. F. (1998), Seafloor tectonic fabric from satellite altimetry, *Annu. Rev. Earth Planet. Sci.*, *26*(1), 697–747, doi:10.1146/annurev.earth.26.1.697.

Smith, W. H. F., and D. T. Sandwell (1997), Global sea floor topography from satellite altimetry and ship depth soundings, *Science*, *277*(5334), 1956–1962, doi:10.1126/science.277.5334.1956.

Taylor, B. (2006), The single largest oceanic plateau: Ontong Java-Manihiki-Hikurangi, *Earth Planet. Sci. Lett.*, *241*(3–4), 372–380, doi:10.1016/j.epsl.2005.11.049.

Veevers, J. J. (2000), Change of tectono-stratigraphic regime in the Australian plate during the 99 Ma (mid-Cretaceous) and 43 Ma (mid-Eocene) swerves of the Pacific, *Geology*, *28*(1), 47–50, doi:10.1130/0091-7613(2000)28<47:COTRIT>2.0.CO;2.

Viso, R. F., R. L. Larson, and R. A. Pockalny (2005), Tectonic evolution of the Pacific-Phoenix-Farallon triple junction in the South Pacific Ocean, *Earth Planet. Sci. Lett.*, *233*(1–2), 179–194, doi:10.1016/j.epsl.2005.02.004.

Wessel, P., and W. F. Haxby (1990), Thermal stresses, differential subsidence, and flexure at oceanic fracture zones, *J. Geophys. Res.*, *95*(B1), 375–391, doi:10.1029/JB095iB01p00375.

Wessel, P., and S. Lyons (1997), Distribution of large Pacific seamounts from Geosat/ERS-1: Implications for the history of intraplate volcanism, *J. Geophys. Res.*, *102*(B10), 22,459–22,475, doi:10.1029/97JB01588.

Wessel, P., and W. H. F. Smith (1998), New, improved version of Generic Mapping Tools released, *Eos Trans. AGU*, *79*(47), 579, doi:10.1029/98EO00426.

West, B. P., J. Lin, and D. M. Christie (1999), Forces driving ridge propagation, *J. Geophys. Res.*, *104*(B10), 22,845–22,858, doi:10.1029/1999JB900154.

Whittaker, J. M., R. D. Müller, G. Leitchenkov, H. Stagg, M. Sdrolias, C. Gaina, and A. Goncharov (2007), Major Australian-Antarctic plate reorganization at Hawaiian-Emperor bend time, *Science*, *318*(5847), 83–86, doi:10.1126/science.1143769.

Whittaker, J. M., R. D. Müller, W. R. Roest, P. Wessel, and W. H. F. Smith (2008), How supercontinents and superoceans affect seafloor roughness, *Nature*, *456*(7224), 938–941, doi:10.1038/nature07573.

Whittaker, J. M., R. D. Müller, and M. Gurnis (2010), Development of the Australian-Antarctic depth anomaly, *Geochem. Geophys. Geosyst.*, *11*, Q11006, doi:10.1029/2010GC003276.

K. J. Matthews, R. D. Müller, and J. M. Whittaker, EarthByte Group, School of Geosciences, University of Sydney, Sydney, NSW 2006, Australia. (kara.matthews@sydney.edu.au)

P. Wessel, School of Ocean and Earth Science and Technology, University of Hawaii at Manoa, 1680 East-West Rd., Honolulu, HI 96822, USA.